Chromenopyrazole-based TADF emitters for bluish-green and sky-blue OLEDs

Vladislav M. Korshunov,*[a,b] Timofey N. Chmovzh,[c] Alisia V. Tsorieva,[a] Ivan A. Zhukov,[c,d,e] Dmitry A. Lypenko,[f] Darina I. Nasyrova[c], Artem V. Dmitriev,[f] Ivan V. Ivanov,[d] Valery F. Traven,[d,e] Ilya V. Taydakov,[a] Oleg A. Rakitin.*[c]

a *P. N. Lebedev Physical Institute of the Russian Academy of Sciences, 53 Leninskiy Prospect, 119991 Moscow, Russia*

b Bauman Moscow State Technical University, 5/1 2-ya Baumanskaya Str., 105005 Moscow, Russia

c *N. D. Zelinsky Institute of Organic Chemistry, Russian Academy of Sciences, Leninsky prospect, 47, Moscow, 119991, Russia.*

d *D. I. Mendeleev University of Chemical Technology of Russia, Miusskaya Pl. 9, 124047 Moscow, Russia*

e Skoltech Center for Energy Science and Technology, Skolkovo Institute of Science and Technology, 121205 Moscow, Russia

f A.N. Frumkin Institute of Physical Chemistry and Electrochemistry, Russian Academy of Sciences, Leninsky Prospect 31, Bld. 4, 119071 Moscow, Russia

Table of contents:

SI-1 NMR spectra

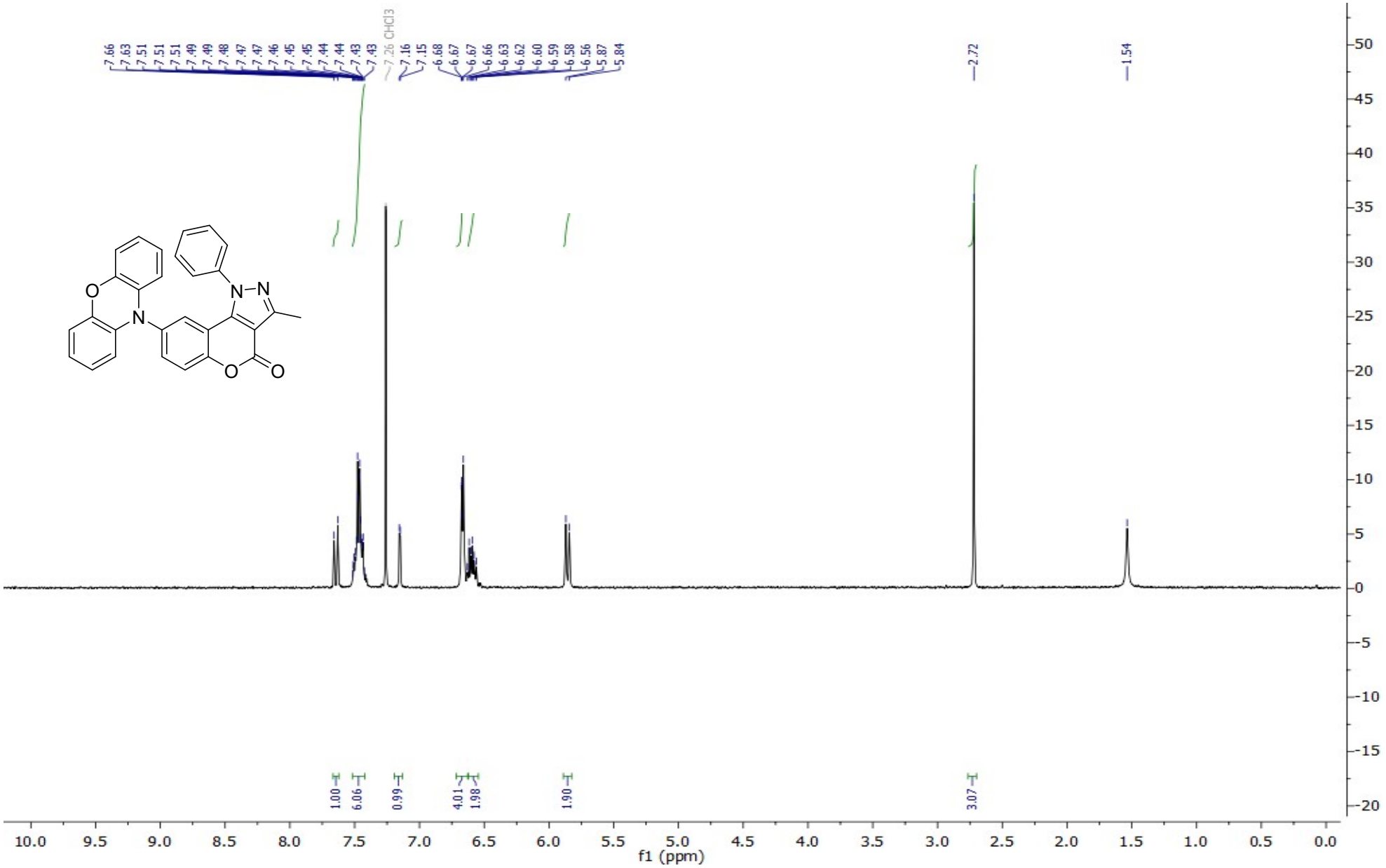

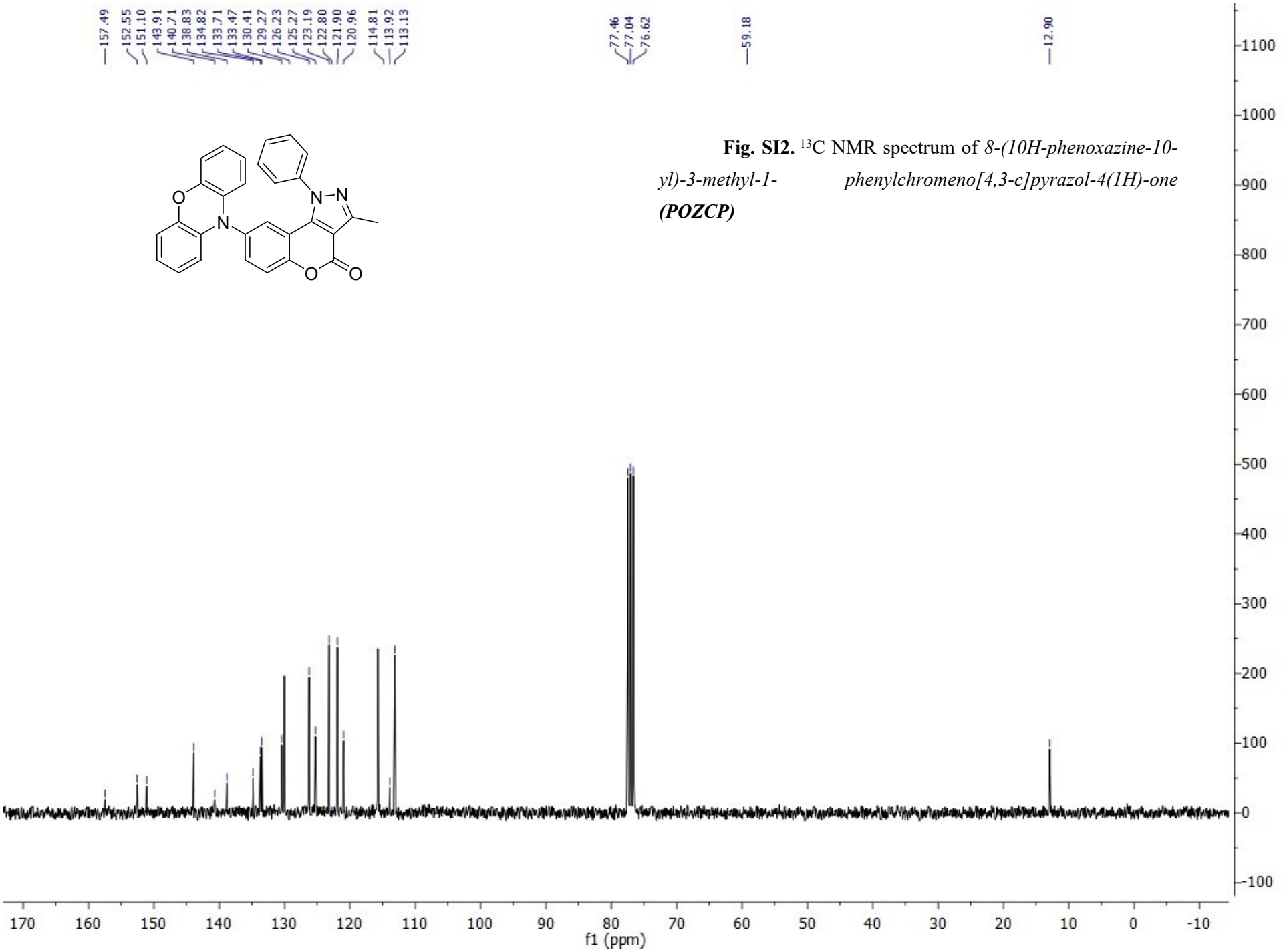

Fig. SI2. ^{13}C NMR spectrum of *8-(10H-phenoxazine-10-yl)-3-methyl-1-phenylchromeno[4,3-c]pyrazol-4(1H)-one* ***(POZCP)***

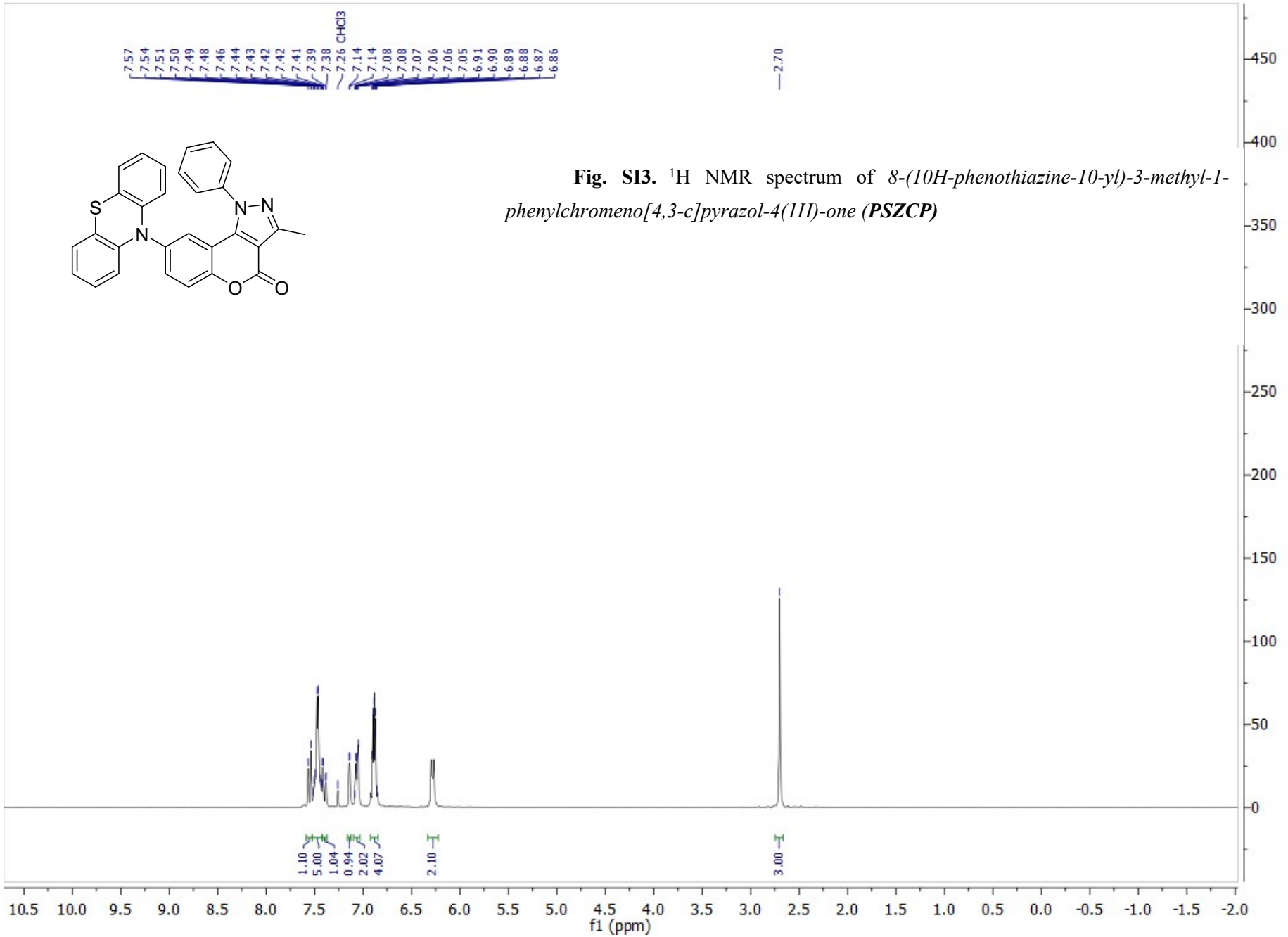

Fig. SI3. ^{1}H NMR spectrum of *8-(10H-phenothiazine-10-yl)-3-methyl-1-phenylchromeno[4,3-c]pyrazol-4(1H)-one* ***(PSZCP)***

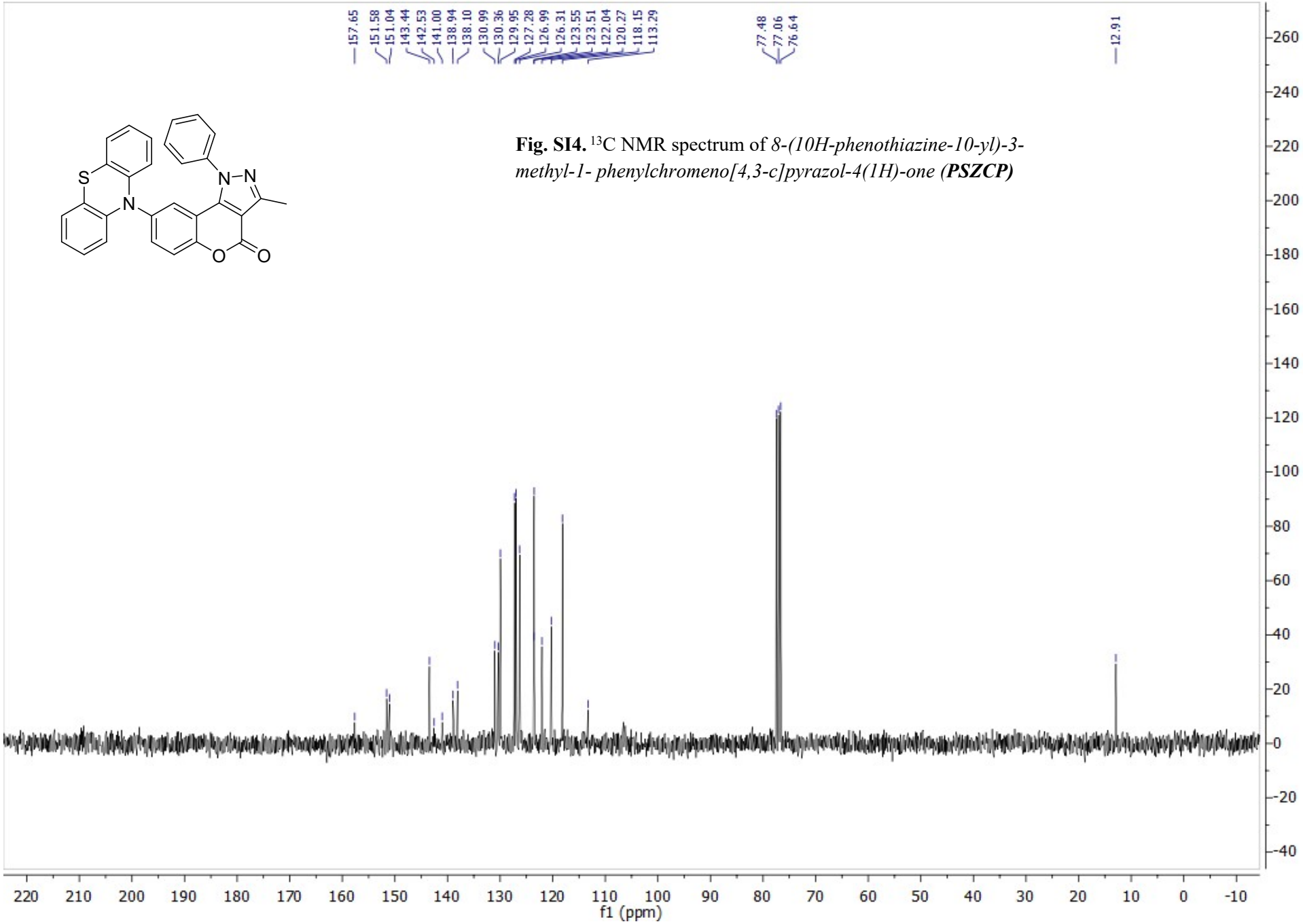

Fig. SI4. ^{13}C NMR spectrum of *8-(10H-phenothiazine-10-yl)-3-methyl-1- phenylchromeno[4,3-c]pyrazol-4(1H)-one* ***(PSZCP)***

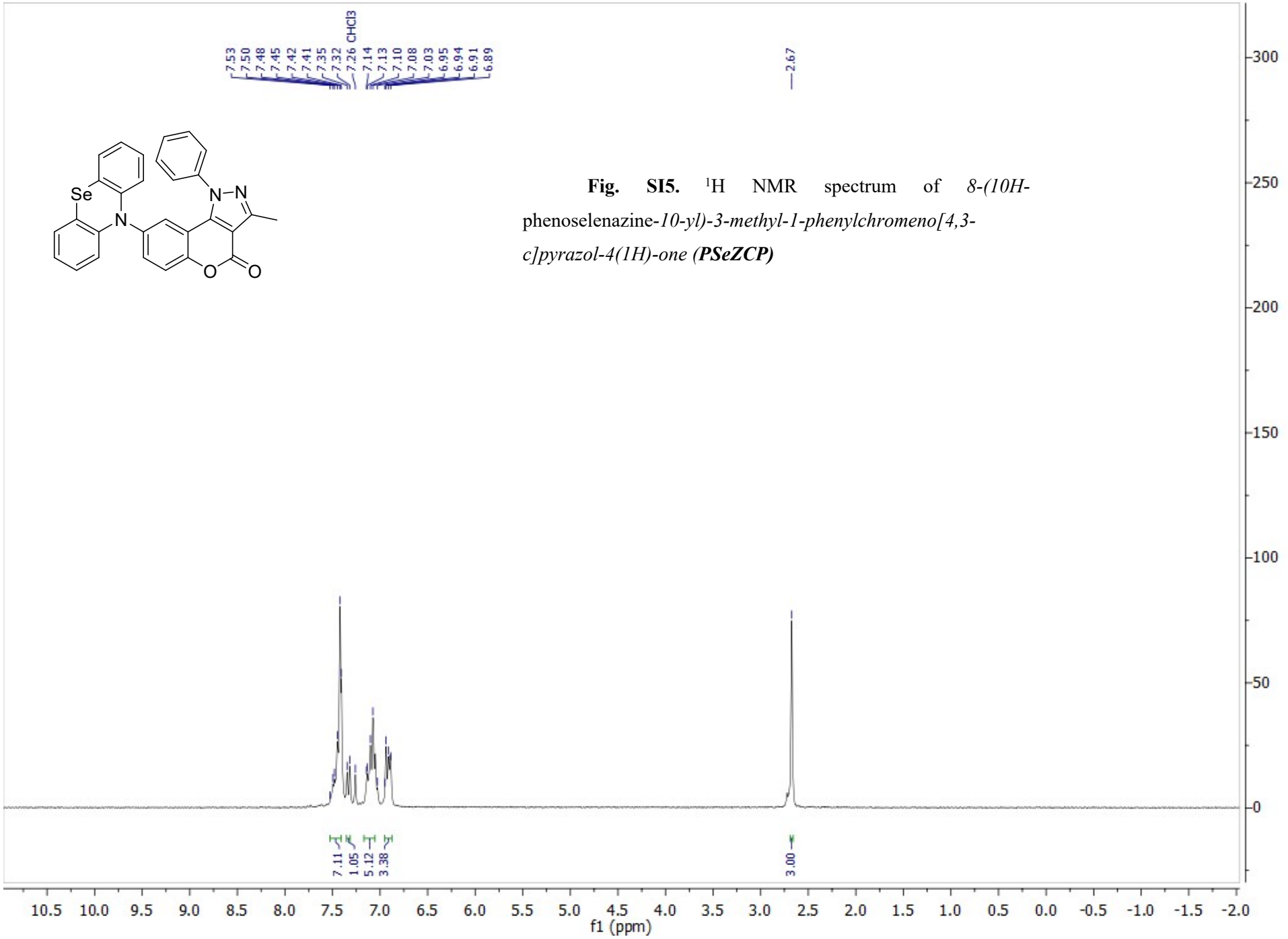

Fig. SI5. ^{1}H NMR spectrum of *8-(10H-phenoselenazine-10-yl)-3-methyl-1-phenylchromeno[4,3-c]pyrazol-4(1H)-one* ***(PSeZCP)***

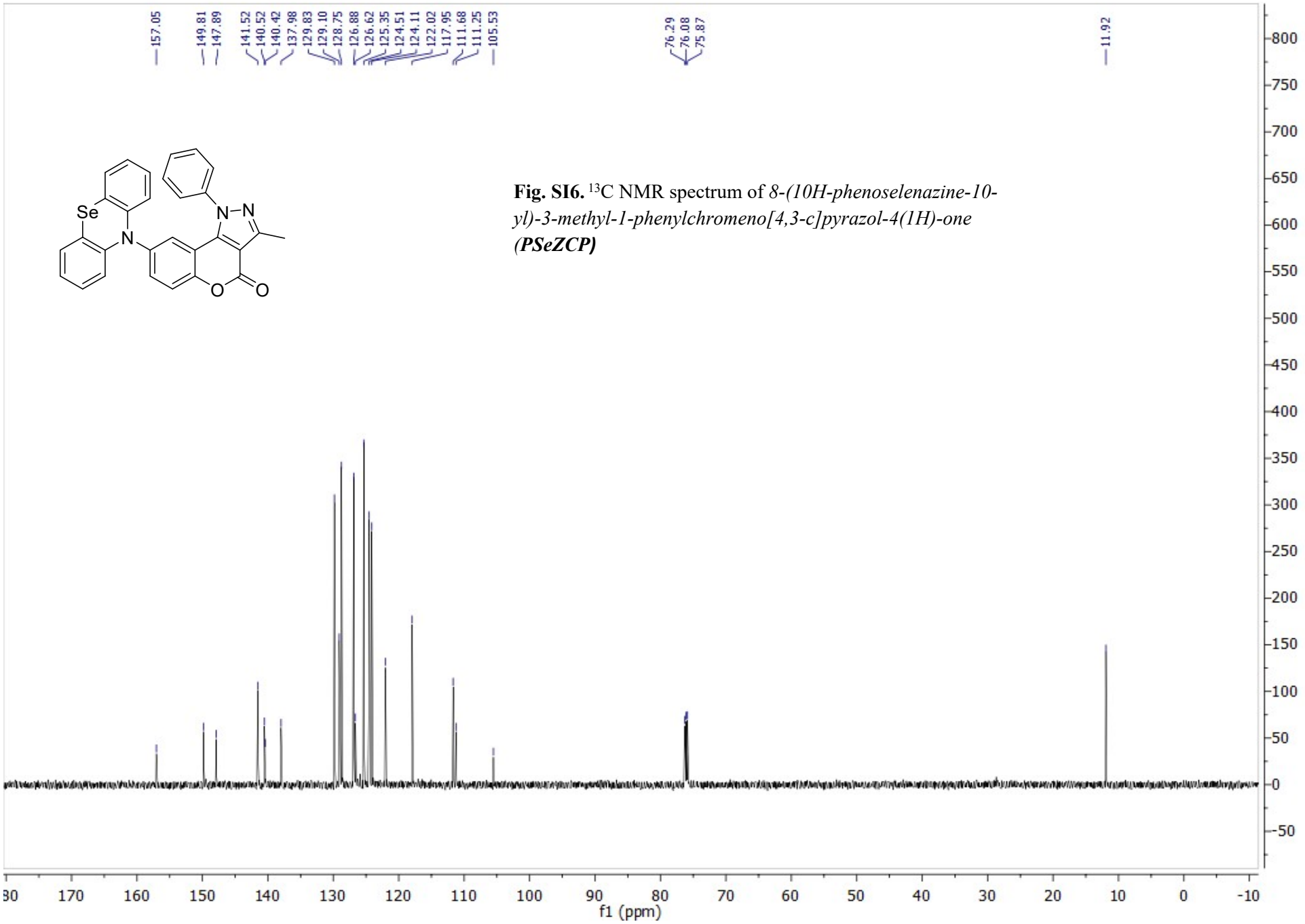

Fig. SI6. ^{13}C NMR spectrum of *8-(10H-phenoselenazine-10-yl)-3-methyl-1-phenylchromeno[4,3-c]pyrazol-4(1H)-one* ***(PSeZCP)***

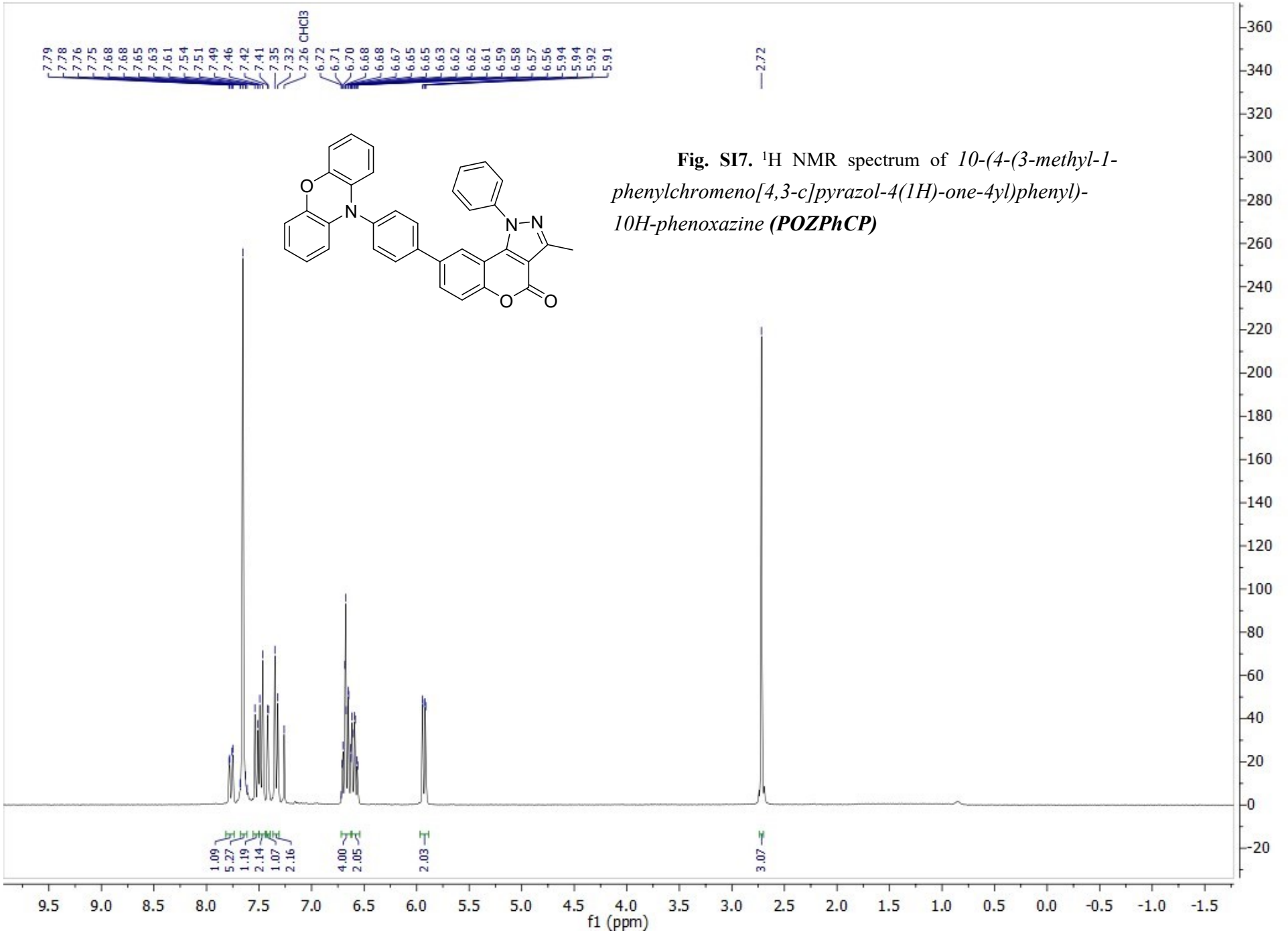

Fig. SI7. ^{1}H NMR spectrum of *10-(4-(3-methyl-1-phenylchromeno[4,3-c]pyrazol-4(1H)-one-4yl)phenyl)-10H-phenoxazine* ***(POZPhCP)***

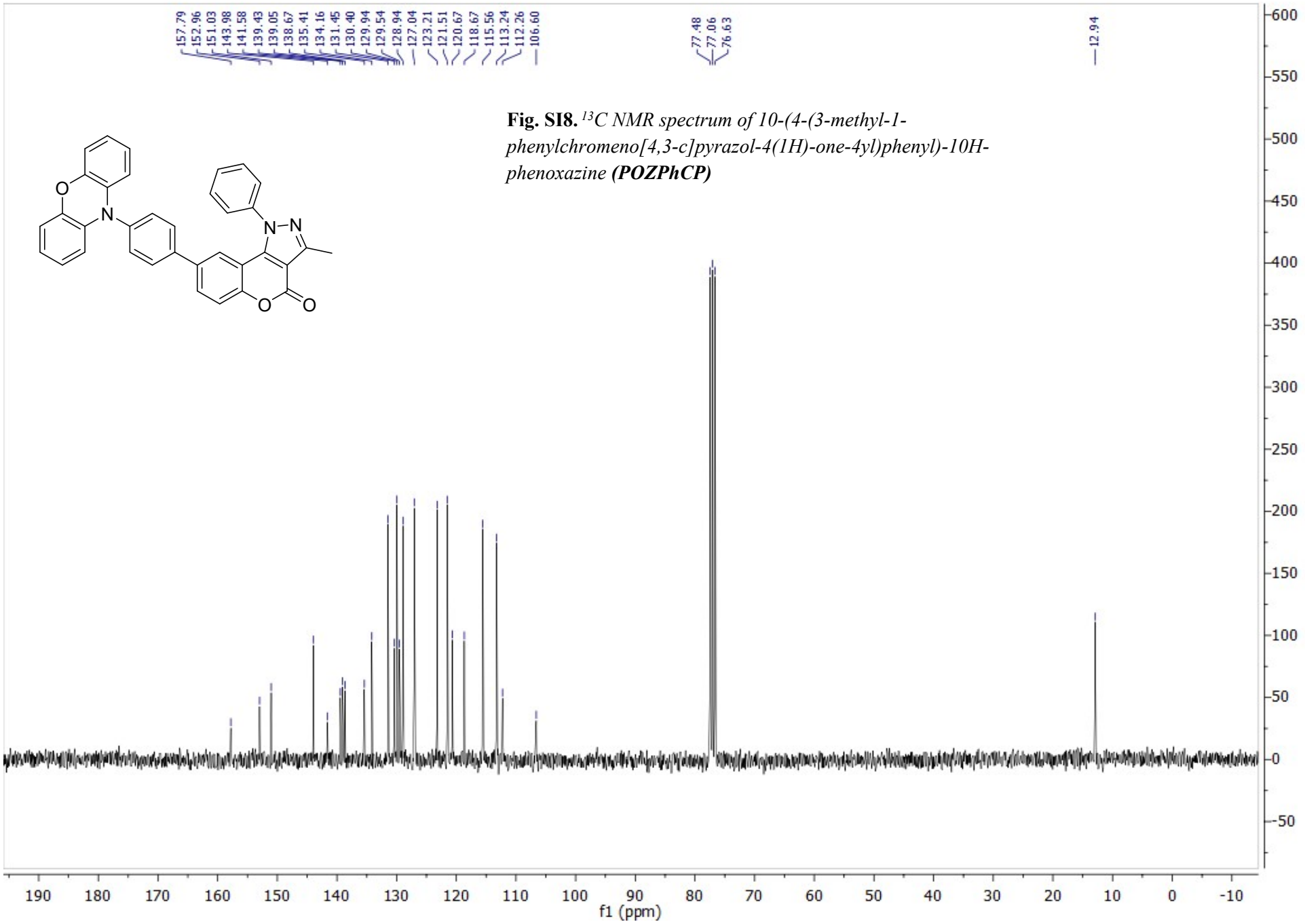

Fig. SI8. *^{13}C NMR spectrum of 10-(4-(3-methyl-1-phenylchromeno[4,3-c]pyrazol-4(1H)-one-4yl)phenyl)-10H-phenoxazine* ***(POZPhCP)***

Molecular design

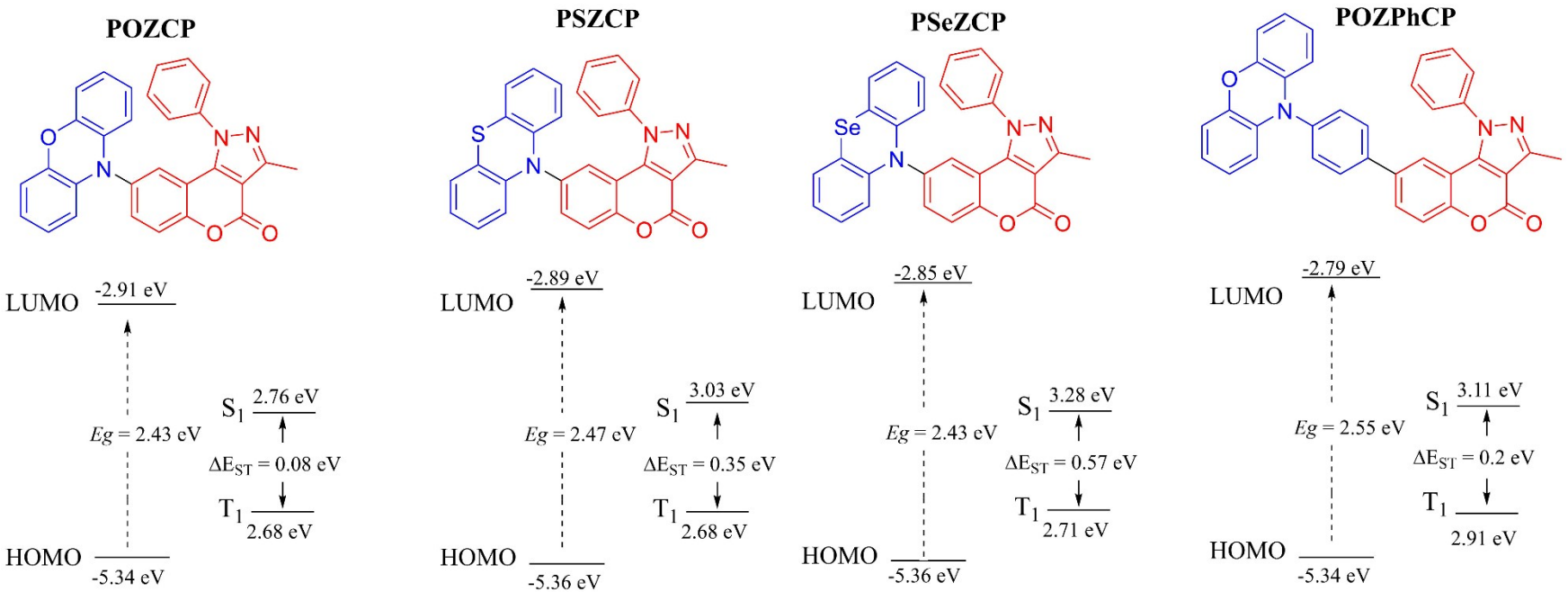

Chemical structures (upper), HOMO and LUMO distributions, and measured singlet (S_1) and triplet (T_1) energy levels (lower) for D–A molecules **(POZCP, PSZCP,PSeZCP and POZPhCP).**

SI-2 X-ray crystallographic data and refinement details.

Crystal data, data collection and structure refinement details are summarized in **Table SI1**.

Table SI1 Crystal data for **POZCP**, **PSZCP**, **PSeZCP**, **POZPhCP**

Compound	**POZCP**	**PSZCP**	**PSeZCP**	**POZPhCP**
Empirical formula	$C_{29}H_{19}N_3O_3$	$C_{29}H_{19}N_3O_2S$	$C_{29}H_{19}N_3O_2Se$	$C_{35}H_{23}N_3O_3$
Formula weight	457.47	473.53	520.43	533.56
Temperature, K	100.00(10)	100.00(10)	100.00(10)	100.00(10)
Wavelength, Å	1.54184	1.54184	1.54184	1.54184
Crystal system	Monoclinic	Monoclinic	Triclinic	Monoclinic
Space group	$P2_1/c$	$P2_1/c$	$P\bar{1}$	$P2_1/n$
Unit cell dimensions				
a, Å	10.00170(10)	17.8600(3)	8.80580(10)	14.9667(3)
b, Å	102.1270(10)	9.42620(10)	10.48780(10)	9.11850(10)
c, Å	6.73430(10)	13.9246(3)	13.7387(2)	18.6135(3)
Volume, $Å^3$	2151.48(5)	2229.94(7)	1128.87(3)	2532.45(7)
Z	4	4	2	4
Density (calcd.), $g{\cdot}cm^{-3}$	1.412	1.410	1.531	1.399
Absorption coefficient, mm^{-1}	0.753	1.564	2.524	0.725
F(000)	952	984	528	1112
Crystal size, mm^3	0.5 x 0.3 x 0.2	0.444 x 0.345 x 0.121	0.28 x 0.09 x 0.07	0.287 x 0.228 x 0.055
Theta range for data collection	2.705 to 80.144°	2.601 to 79.751°	3.359 to 80.309°	3.653 to 79.936°
Reflections collected	25650	8656	2984	55392
Independent [R_{int}]	4635 [0.0264]	8656	4901 [0.0360]	5392
Completeness to theta = 67.684°	99.9 %	100.0 %	100.0 %	99.5 %
Data / restraints / parameters	4635 / 57 / 360	8656 / 0 / 318	4901 / 0 / 317	5392 / 0 / 372
Goodness-of-fit on F^2	1.066	1.067	1.041	1.064
R_1 / wR_2 for I>2s(I)	0.0400 / 0.1074	0.0444 / 0.1294	0.0309 / 0.0822	0.0627 / 0.1716

R_1 / wR_2 (all reflections)	0.0418 / 0.1089	0.0454 / 0.1303	0.0316 / 0.0827	0.0726 / 0.1792
R_{max}/r_{min}, e.Å^{-3}	0.180 and -0.179	0.248 and -0.479	0.736 and -0.605	0.361 and -0.206
CCDC number	2474440	2474441	2474212	2474213

Crystal structure of POZCP

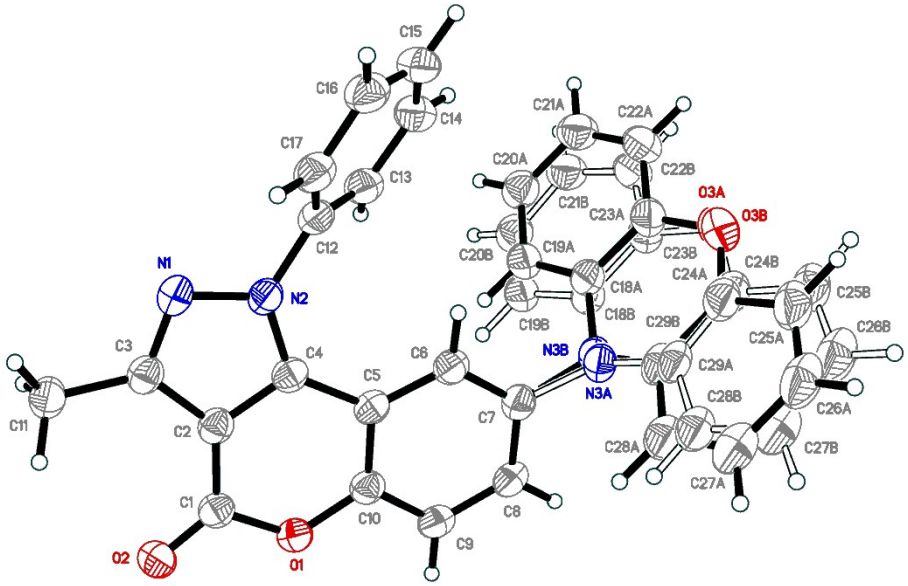

Figure SI1. The structure of **POZCP** with numeration of the non-hydrogen atoms. Thermal ellipsoids are set to the 50% probability level.

Table SI2. Selected bond length (Å) and angle (°) in the crystals for compound **POZCP**.

Bond length (Å)			
O(1)-C(1)	1.3872(15)	O(3A)-C(24A)	1.3844(19)
O(1)-C(10)	1.3816(14)	C(18A)-C(19A)	1.3932(19)
N(1)-N(2)	1.3797(14)	C(18A)-C(23A)	1.3965(18)
N(1)-C(3)	1.3235(16)	C(19A)-C(20A)	1.3880(19)
C(1)-O(2)	1.2055(15)	C(20A)-C(21A)	1.383(2)
C(1)-C(2)	1.4405(17)	C(21A)-C(22A)	1.387(2)
N(2)-C(4)	1.3531(15)	C(22A)-C(23A)	1.379(2)
N(2)-C(12)	1.4376(16)	C(24A)-C(25A)	1.386(2)
C(2)-C(3)	1.4142(16)	C(24A)-C(29A)	1.396(2)
C(2)-C(4)	1.3843(17)	C(25A)-C(26A)	1.385(3)
C(3)-C(11)	1.4962(17)	C(26A)-C(27A)	1.381(2)
C(4)-C(5)	1.4498(16)	C(27A)-C(28A)	1.394(2)
C(5)-C(6)	1.3938(17)	C(28A)-C(29A)	1.391(2)
C(5)-C(10)	1.4071(17)	N(3B)-C(18B)	1.416(3)
C(6)-C(7)	1.3848(17)	N(3B)-C(29B)	1.418(3)
C(7)-C(8)	1.3943(17)	O(3B)-C(23B)	1.385(4)
C(7)-N(3A)	1.4369(16)	O(3B)-C(24B)	1.375(5)
C(7)-N(3B)	1.440(3)	C(18B)-C(19B)	1.394(3)
C(8)-C(9)	1.3861(18)	C(18B)-C(23B)	1.395(3)
C(9)-C(10)	1.3883(17)	C(19B)-C(20B)	1.388(3)

C(12)-C(13)	1.3872(18)	C(20B)-C(21B)	1.383(3)
C(12)-C(17)	1.3863(17)	C(21B)-C(22B)	1.388(3)
C(13)-C(14)	1.3890(18)	C(22B)-C(23B)	1.379(3)
C(14)-C(15)	1.393(2)	C(24B)-C(25B)	1.386(3)
C(15)-C(16)	1.386(2)	C(24B)-C(29B)	1.395(3)
C(16)-C(17)	1.3870(19)	C(25B)-C(26B)	1.385(4)
N(3A)-C(18A)	1.4187(17)	C(26B)-C(27B)	1.381(4)
N(3A)-C(29A)	1.4193(16)	C(27B)-C(28B)	1.394(3)
O(3A)-C(23A)	1.3855(17)	C(28B)-C(29B)	1.393(3)

Angles (°)			
C(10)-O(1)-C(1)	123.04(9)	C(24A)-O(3A)-C(23A)	116.90(11)
C(3)-N(1)-N(2)	106.17(10)	C(19A)-C(18A)-N(3A)	122.03(12)
O(1)-C(1)-C(2)	114.97(10)	C(19A)-C(18A)-C(23A)	118.04(13)
O(2)-C(1)-O(1)	117.14(11)	C(23A)-C(18A)-N(3A)	119.87(12)
O(2)-C(1)-C(2)	127.88(12)	C(20A)-C(19A)-C(18A)	120.80(13)
N(1)-N(2)-C(12)	118.59(9)	C(21A)-C(20A)-C(19A)	120.40(14)
C(4)-N(2)-N(1)	111.10(10)	C(20A)-C(21A)-C(22A)	119.28(14)
C(4)-N(2)-C(12)	130.31(10)	C(23A)-C(22A)-C(21A)	120.38(14)
C(3)-C(2)-C(1)	131.14(11)	O(3A)-C(23A)-C(18A)	121.82(13)
C(4)-C(2)-C(1)	122.81(11)	C(22A)-C(23A)-O(3A)	117.09(13)
C(4)-C(2)-C(3)	106.04(10)	C(22A)-C(23A)-C(18A)	121.07(13)
N(1)-C(3)-C(2)	110.12(11)	O(3A)-C(24A)-C(25A)	116.56(14)
N(1)-C(3)-C(11)	121.33(11)	O(3A)-C(24A)-C(29A)	122.29(13)
C(2)-C(3)-C(11)	128.51(11)	C(25A)-C(24A)-C(29A)	121.14(15)
N(2)-C(4)-C(2)	106.56(10)	C(26A)-C(25A)-C(24A)	119.73(15)
N(2)-C(4)-C(5)	132.51(11)	C(27A)-C(26A)-C(25A)	120.11(14)
C(2)-C(4)-C(5)	120.93(11)	C(26A)-C(27A)-C(28A)	119.96(16)
C(6)-C(5)-C(4)	127.58(11)	C(29A)-C(28A)-C(27A)	120.74(14)
C(6)-C(5)-C(10)	117.68(11)	C(24A)-C(29A)-N(3A)	119.47(13)
C(10)-C(5)-C(4)	114.73(11)	C(28A)-C(29A)-N(3A)	122.22(12)
C(7)-C(6)-C(5)	121.00(11)	C(28A)-C(29A)-C(24A)	118.30(13)
C(6)-C(7)-C(8)	120.56(12)	C(18B)-N(3B)-C(7)	101.0(11)
C(6)-C(7)-N(3A)	118.58(11)	C(18B)-N(3B)-C(29B)	117.4(2)
C(6)-C(7)-N(3B)	118.2(2)	C(29B)-N(3B)-C(7)	139.4(15)
C(8)-C(7)-N(3A)	120.84(11)	C(24B)-O(3B)-C(23B)	117.4(3)
C(8)-C(7)-N(3B)	120.4(2)	C(19B)-C(18B)-N(3B)	121.6(4)
C(9)-C(8)-C(7)	119.26(11)	C(19B)-C(18B)-C(23B)	118.0(3)
C(8)-C(9)-C(10)	120.05(11)	C(23B)-C(18B)-N(3B)	120.3(3)
O(1)-C(10)-C(5)	123.32(11)	C(20B)-C(19B)-C(18B)	120.7(3)
O(1)-C(10)-C(9)	115.43(10)	C(21B)-C(20B)-C(19B)	120.4(3)

C(9)-C(10)-C(5)	121.25(11)	C(20B)-C(21B)-C(22B)	119.2(3)
C(13)-C(12)-N(2)	119.62(11)	C(23B)-C(22B)-C(21B)	120.3(3)
C(17)-C(12)-N(2)	118.83(11)	O(3B)-C(23B)-C(18B)	122.1(4)
C(17)-C(12)-C(13)	121.55(12)	C(22B)-C(23B)-O(3B)	116.6(6)
C(12)-C(13)-C(14)	118.83(12)	C(22B)-C(23B)-C(18B)	121.1(3)
C(13)-C(14)-C(15)	120.28(13)	O(3B)-C(24B)-C(25B)	115.8(4)
C(16)-C(15)-C(14)	119.80(13)	O(3B)-C(24B)-C(29B)	123.0(3)
C(15)-C(16)-C(17)	120.54(13)	C(25B)-C(24B)-C(29B)	121.2(3)
C(12)-C(17)-C(16)	118.89(13)	C(26B)-C(25B)-C(24B)	119.8(3)
C(18A)-N(3A)-C(7)	116.59(10)	C(27B)-C(26B)-C(25B)	120.0(4)
C(18A)-N(3A)-C(29A)	116.92(11)	C(26B)-C(27B)-C(28B)	120.0(4)
C(29A)-N(3A)-C(7)	116.90(11)	C(29B)-C(28B)-C(27B)	120.7(3)

Crystal structure of PSZCP

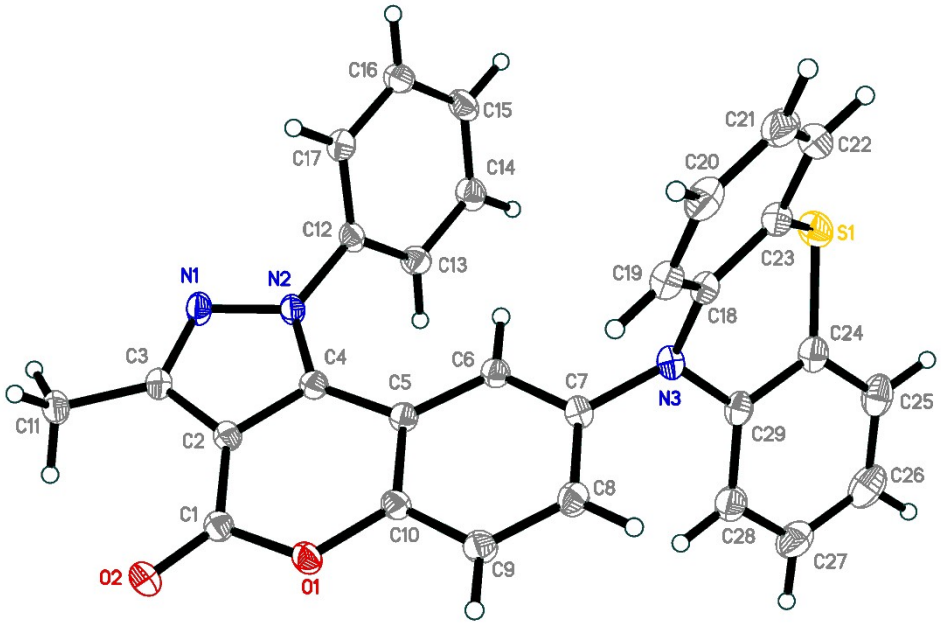

Figure SI2. The structure of **PSZCP** with numeration of the non-hydrogen atoms. Thermal ellipsoids are set to the 50% probability level.

Table SI3. Selected bond length (Å) and angle (°) in the crystals for compound **PSZCP**.

Bond length (Å)			
S(1)-C(23)	1.7611(19)	C(8)-C(9)	1.385(2)
S(1)-C(24)	1.7624(19)	C(9)-C(10)	1.391(2)
O(1)-C(1)	1.3861(19)	C(12)-C(13)	1.388(2)
O(1)-C(10)	1.3831(18)	C(12)-C(17)	1.390(2)
O(2)-C(1)	1.2064(19)	C(13)-C(14)	1.395(2)
N(1)-N(2)	1.3813(18)	C(14)-C(15)	1.387(3)
N(1)-C(3)	1.328(2)	C(15)-C(16)	1.388(3)

N(2)-C(4)	1.350(2)	C(16)-C(17)	1.396(2)
N(2)-C(12)	1.4403(19)	C(18)-C(19)	1.392(2)
N(3)-C(7)	1.4412(19)	C(18)-C(23)	1.400(2)
N(3)-C(18)	1.423(2)	C(19)-C(20)	1.389(3)
N(3)-C(29)	1.417(2)	C(20)-C(21)	1.383(3)
C(1)-C(2)	1.434(2)	C(21)-C(22)	1.388(3)
C(2)-C(3)	1.417(2)	C(22)-C(23)	1.392(3)
C(2)-C(4)	1.391(2)	C(24)-C(25)	1.393(3)
C(3)-C(11)	1.496(2)	C(24)-C(29)	1.405(2)
C(4)-C(5)	1.447(2)	C(25)-C(26)	1.381(3)
C(5)-C(6)	1.408(2)	C(26)-C(27)	1.388(3)
C(5)-C(10)	1.406(2)	C(27)-C(28)	1.395(3)
C(6)-C(7)	1.385(2)	C(28)-C(29)	1.394(2)
C(7)-C(8)	1.396(2)		

Angles (°)			
C(23)-S(1)-C(24)	98.75(8)	O(1)-C(10)-C(9)	115.08(13)
C(10)-O(1)-C(1)	122.99(12)	C(9)-C(10)-C(5)	121.47(15)
C(3)-N(1)-N(2)	105.71(13)	C(13)-C(12)-N(2)	119.12(15)
N(1)-N(2)-C(12)	118.74(13)	C(13)-C(12)-C(17)	121.91(15)
C(4)-N(2)-N(1)	111.80(12)	C(17)-C(12)-N(2)	118.97(15)
C(4)-N(2)-C(12)	129.46(13)	C(12)-C(13)-C(14)	118.73(16)
C(18)-N(3)-C(7)	116.97(14)	C(15)-C(14)-C(13)	120.05(16)
C(29)-N(3)-C(7)	119.25(14)	C(14)-C(15)-C(16)	120.64(15)
C(29)-N(3)-C(18)	119.25(13)	C(15)-C(16)-C(17)	120.05(16)
O(1)-C(1)-C(2)	115.12(13)	C(12)-C(17)-C(16)	118.60(16)
O(2)-C(1)-O(1)	117.05(14)	C(19)-C(18)-N(3)	121.81(15)
O(2)-C(1)-C(2)	127.83(15)	C(19)-C(18)-C(23)	118.87(16)
C(3)-C(2)-C(1)	131.25(14)	C(23)-C(18)-N(3)	119.32(15)
C(4)-C(2)-C(1)	122.74(14)	C(20)-C(19)-C(18)	120.13(17)
C(4)-C(2)-C(3)	106.00(14)	C(21)-C(20)-C(19)	121.05(17)
N(1)-C(3)-C(2)	110.24(14)	C(20)-C(21)-C(22)	119.26(17)
N(1)-C(3)-C(11)	121.71(15)	C(21)-C(22)-C(23)	120.23(17)
C(2)-C(3)-C(11)	128.04(15)	C(18)-C(23)-S(1)	119.24(14)
N(2)-C(4)-C(2)	106.25(14)	C(22)-C(23)-S(1)	120.29(13)
N(2)-C(4)-C(5)	132.68(14)	C(22)-C(23)-C(18)	120.45(17)
C(2)-C(4)-C(5)	121.05(14)	C(25)-C(24)-S(1)	119.50(14)
C(6)-C(5)-C(4)	127.46(14)	C(25)-C(24)-C(29)	120.79(17)
C(10)-C(5)-C(4)	114.65(14)	C(29)-C(24)-S(1)	119.37(13)
C(10)-C(5)-C(6)	117.89(14)	C(26)-C(25)-C(24)	120.38(17)
C(7)-C(6)-C(5)	120.56(14)	C(25)-C(26)-C(27)	119.27(17)

C(6)-C(7)-N(3)	117.68(14)	C(26)-C(27)-C(28)	120.83(18)
C(6)-C(7)-C(8)	120.46(14)	C(29)-C(28)-C(27)	120.34(17)
C(8)-C(7)-N(3)	121.85(15)	C(24)-C(29)-N(3)	118.80(15)
C(9)-C(8)-C(7)	120.02(15)	C(28)-C(29)-N(3)	122.91(15)
C(8)-C(9)-C(10)	119.57(15)	C(28)-C(29)-C(24)	118.26(16)
O(1)-C(10)-C(5)	123.44(14)		

Crystal structure of PSeZCP

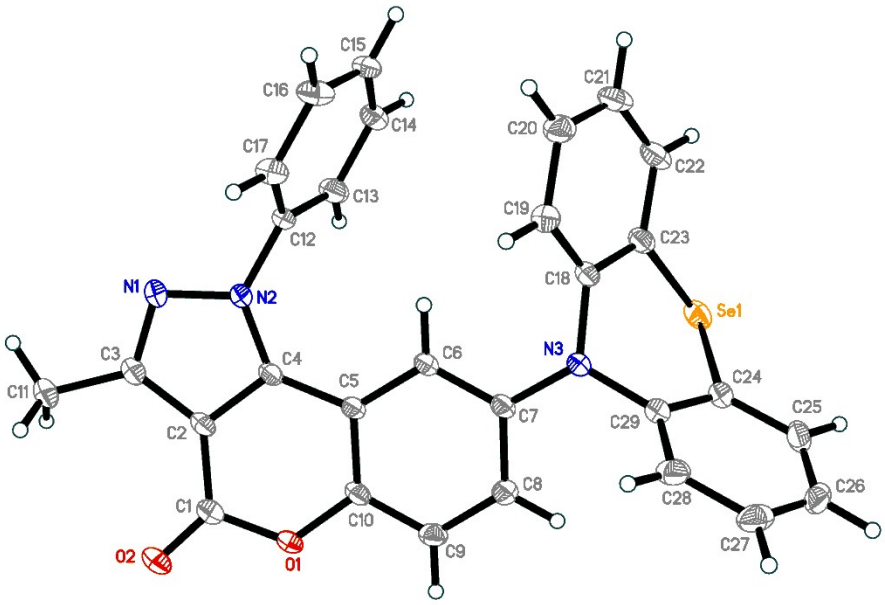

Figure SI3. The structure of **PSeZCP** with numeration of the non-hydrogen atoms. Thermal ellipsoids are set to the 50% probability level.

Table SI4. Selected bond length (Å) and angle (°) in the crystals for compound **PSeZCP**.

Bond length (Å)			
Se(1)-C(23)	1.9123(18)	C(8)-C(9)	1.382(2)
Se(1)-C(24)	1.9127(19)	C(9)-C(10)	1.385(2)
O(1)-C(1)	1.386(2)	C(12)-C(13)	1.388(2)
O(1)-C(10)	1.3889(19)	C(12)-C(17)	1.385(2)
O(2)-C(1)	1.206(2)	C(13)-C(14)	1.392(2)
N(1)-N(2)	1.3847(19)	C(14)-C(15)	1.382(3)
N(1)-C(3)	1.325(2)	C(15)-C(16)	1.389(3)
N(2)-C(4)	1.348(2)	C(16)-C(17)	1.390(2)
N(2)-C(12)	1.432(2)	C(18)-C(19)	1.394(3)
N(3)-C(7)	1.406(2)	C(18)-C(23)	1.393(2)
N(3)-C(18)	1.427(2)	C(19)-C(20)	1.390(3)
N(3)-C(29)	1.428(2)	C(20)-C(21)	1.387(3)
C(1)-C(2)	1.439(2)	C(21)-C(22)	1.386(3)
C(2)-C(3)	1.416(2)	C(22)-C(23)	1.395(2)

C(2)-C(4)	1.392(2)	C(24)-C(25)	1.391(2)
C(3)-C(11)	1.490(2)	C(24)-C(29)	1.392(3)
C(4)-C(5)	1.448(2)	C(25)-C(26)	1.369(3)
C(5)-C(6)	1.407(2)	C(26)-C(27)	1.402(3)
C(5)-C(10)	1.402(2)	C(27)-C(28)	1.393(3)
C(6)-C(7)	1.393(2)	C(28)-C(29)	1.400(3)
C(7)-C(8)	1.410(2)		

Angles (°)			
C(23)-Se(1)-C(24)	93.34(8)	O(1)-C(10)-C(5)	123.53(15)
C(1)-O(1)-C(10)	123.33(13)	C(9)-C(10)-O(1)	115.85(14)
C(3)-N(1)-N(2)	105.56(14)	C(9)-C(10)-C(5)	120.61(15)
N(1)-N(2)-C(12)	118.11(13)	C(13)-C(12)-N(2)	119.90(15)
C(4)-N(2)-N(1)	111.84(13)	C(17)-C(12)-N(2)	118.56(15)
C(4)-N(2)-C(12)	130.05(14)	C(17)-C(12)-C(13)	121.54(16)
C(7)-N(3)-C(18)	123.24(14)	C(12)-C(13)-C(14)	118.85(16)
C(7)-N(3)-C(29)	120.93(14)	C(15)-C(14)-C(13)	120.18(17)
C(18)-N(3)-C(29)	115.20(14)	C(14)-C(15)-C(16)	120.39(16)
O(1)-C(1)-C(2)	114.63(14)	C(15)-C(16)-C(17)	120.07(17)
O(2)-C(1)-O(1)	116.96(16)	C(12)-C(17)-C(16)	118.96(17)
O(2)-C(1)-C(2)	128.42(17)	C(19)-C(18)-N(3)	121.41(16)
C(3)-C(2)-C(1)	131.52(16)	C(23)-C(18)-N(3)	119.21(16)
C(4)-C(2)-C(1)	122.54(16)	C(23)-C(18)-C(19)	119.14(16)
C(4)-C(2)-C(3)	105.93(14)	C(20)-C(19)-C(18)	120.21(17)
N(1)-C(3)-C(2)	110.45(15)	C(21)-C(20)-C(19)	120.16(18)
N(1)-C(3)-C(11)	121.05(16)	C(22)-C(21)-C(20)	120.27(17)
C(2)-C(3)-C(11)	128.50(16)	C(21)-C(22)-C(23)	119.48(18)
N(2)-C(4)-C(2)	106.22(14)	C(18)-C(23)-Se(1)	117.61(13)
N(2)-C(4)-C(5)	132.11(15)	C(18)-C(23)-C(22)	120.70(17)
C(2)-C(4)-C(5)	121.61(15)	C(22)-C(23)-Se(1)	121.55(14)
C(6)-C(5)-C(4)	126.62(15)	C(25)-C(24)-Se(1)	121.60(15)
C(10)-C(5)-C(4)	114.16(15)	C(25)-C(24)-C(29)	120.56(18)
C(10)-C(5)-C(6)	119.15(15)	C(29)-C(24)-Se(1)	117.79(13)
C(7)-C(6)-C(5)	120.56(15)	C(26)-C(25)-C(24)	119.70(19)
N(3)-C(7)-C(8)	119.48(15)	C(25)-C(26)-C(27)	120.62(17)
C(6)-C(7)-N(3)	121.93(15)	C(28)-C(27)-C(26)	120.02(19)
C(6)-C(7)-C(8)	118.58(15)	C(27)-C(28)-C(29)	119.14(19)
C(9)-C(8)-C(7)	121.20(16)	C(24)-C(29)-N(3)	119.03(16)
C(8)-C(9)-C(10)	119.69(15)	C(24)-C(29)-C(28)	119.88(17)

Crystal structure of POZPhCP

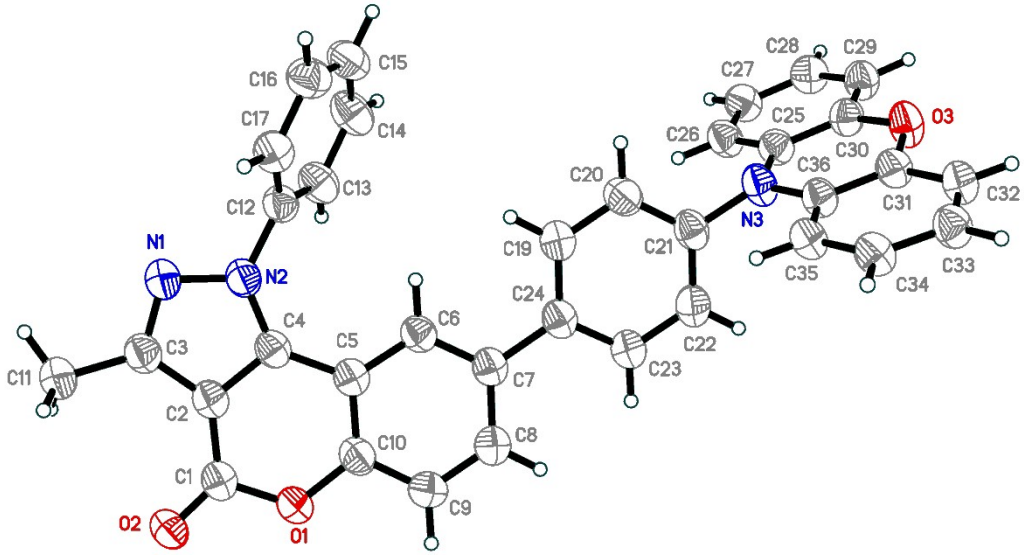

Figure SI4. The structure of **POZPhCP** with numeration of the non-hydrogen atoms. Thermal ellipsoids are set to the 50% probability level. The disorder is omitted.

Table SI5. Selected bond length (Å) and angle (°) in the crystals for compound **POZPhCP**.

Bond length (Å)			
O(1)-C(1)	1.386(3)	C(12)-C(13)	1.369(3)
O(1)-C(10)	1.385(2)	C(12)-C(17)	1.386(3)
O(2)-C(1)	1.206(2)	C(13)-C(14)	1.387(3)
O(3)-C(30)	1.391(2)	C(14)-C(15)	1.372(4)
O(3)-C(31)	1.384(2)	C(15)-C(16)	1.386(4)
N(1)-N(2)	1.378(2)	C(16)-C(17)	1.387(3)
N(1)-C(3)	1.320(3)	C(19)-C(20)	1.388(3)
N(2)-C(4)	1.345(3)	C(19)-C(24)	1.392(3)
N(2)-C(12)	1.437(3)	C(20)-C(21)	1.381(3)
N(3)-C(21)	1.440(3)	C(21)-C(22)	1.379(3)
N(3)-C(25)	1.397(3)	C(22)-C(23)	1.387(3)
N(3)-C(36)	1.409(3)	C(23)-C(24)	1.393(3)
C(1)-C(2)	1.435(3)	C(25)-C(26)	1.395(3)
C(2)-C(3)	1.411(3)	C(25)-C(30)	1.396(3)
C(2)-C(4)	1.388(3)	C(26)-C(27)	1.385(3)
C(3)-C(11)	1.494(3)	C(27)-C(28)	1.378(3)
C(4)-C(5)	1.456(3)	C(28)-C(29)	1.392(3)
C(5)-C(6)	1.399(3)	C(29)-C(30)	1.372(3)
C(5)-C(10)	1.392(3)	C(31)-C(32)	1.383(3)
C(6)-C(7)	1.390(3)	C(31)-C(36)	1.398(3)
C(7)-C(8)	1.400(3)	C(32)-C(33)	1.386(3)
C(7)-C(24)	1.493(3)	C(33)-C(34)	1.382(3)

C(8)-C(9)	1.379(3)	C(34)-C(35)	1.393(3)
C(9)-C(10)	1.383(3)	C(35)-C(36)	1.389(3)

Angles (°)			
C(10)-O(1)-C(1)	122.99(16)	C(17)-C(12)-N(2)	119.03(19)
C(31)-O(3)-C(30)	117.48(16)	C(12)-C(13)-C(14)	119.3(2)
C(3)-N(1)-N(2)	105.80(17)	C(15)-C(14)-C(13)	120.7(2)
N(1)-N(2)-C(12)	117.64(17)	C(14)-C(15)-C(16)	119.7(2)
C(4)-N(2)-N(1)	111.69(16)	C(15)-C(16)-C(17)	120.2(2)
C(4)-N(2)-C(12)	130.44(17)	C(12)-C(17)-C(16)	119.1(2)
C(25)-N(3)-C(21)	120.53(17)	C(20)-C(19)-C(24)	121.5(2)
C(25)-N(3)-C(36)	118.89(17)	C(21)-C(20)-C(19)	120.2(2)
C(36)-N(3)-C(21)	118.34(17)	C(20)-C(21)-N(3)	120.0(2)
O(1)-C(1)-C(2)	115.20(17)	C(22)-C(21)-N(3)	120.7(2)
O(2)-C(1)-O(1)	117.04(19)	C(22)-C(21)-C(20)	119.29(19)
O(2)-C(1)-C(2)	127.8(2)	C(21)-C(22)-C(23)	120.3(2)
C(3)-C(2)-C(1)	131.46(19)	C(22)-C(23)-C(24)	121.4(2)
C(4)-C(2)-C(1)	122.59(19)	C(19)-C(24)-C(7)	121.38(19)
C(4)-C(2)-C(3)	105.95(18)	C(19)-C(24)-C(23)	117.18(19)
N(1)-C(3)-C(2)	110.33(18)	C(23)-C(24)-C(7)	121.44(19)
N(1)-C(3)-C(11)	121.1(2)	C(26)-C(25)-N(3)	122.66(19)
C(2)-C(3)-C(11)	128.5(2)	C(26)-C(25)-C(30)	117.51(19)
N(2)-C(4)-C(2)	106.23(17)	C(30)-C(25)-N(3)	119.83(18)
N(2)-C(4)-C(5)	132.83(18)	C(27)-C(26)-C(25)	121.0(2)
C(2)-C(4)-C(5)	120.86(19)	C(28)-C(27)-C(26)	120.6(2)
C(6)-C(5)-C(4)	126.73(19)	C(27)-C(28)-C(29)	118.9(2)
C(10)-C(5)-C(4)	114.83(18)	C(30)-C(29)-C(28)	120.4(2)
C(10)-C(5)-C(6)	118.42(19)	O(3)-C(30)-C(25)	121.91(19)
C(7)-C(6)-C(5)	122.15(19)	C(29)-C(30)-O(3)	116.62(18)
C(6)-C(7)-C(8)	117.32(19)	C(29)-C(30)-C(25)	121.46(19)
C(6)-C(7)-C(24)	120.69(19)	O(3)-C(31)-C(36)	122.19(18)
C(8)-C(7)-C(24)	121.99(19)	C(32)-C(31)-O(3)	116.78(18)
C(9)-C(8)-C(7)	121.6(2)	C(32)-C(31)-C(36)	121.02(19)
C(8)-C(9)-C(10)	119.9(2)	C(31)-C(32)-C(33)	119.93(19)
O(1)-C(10)-C(5)	123.51(19)	C(34)-C(33)-C(32)	119.74(19)
C(9)-C(10)-O(1)	115.90(19)	C(33)-C(34)-C(35)	120.3(2)
C(9)-C(10)-C(5)	120.6(2)	C(36)-C(35)-C(34)	120.50(19)
C(13)-C(12)-N(2)	119.9(2)	C(31)-C(36)-N(3)	119.30(18)
C(13)-C(12)-C(17)	121.1(2)	C(35)-C(36)-N(3)	122.30(18)
		C(35)-C(36)-C(31)	118.39(18)

Structural features

In **POZCP**, the chromenopyrazole core generally deviates from the plane within 2.5 degrees°. A significant deviation is observed for the C10-C5-C6-C7 fragment with the torsion angle of 5.17(17)° and the C2-C4-C5-C10 fragment with the torsion angle of 4.64(16)°. The methyl and carbonyl groups deviate from the chromenopyrazole plane by -0.7(2)° and -2.2(2)°, respectively.

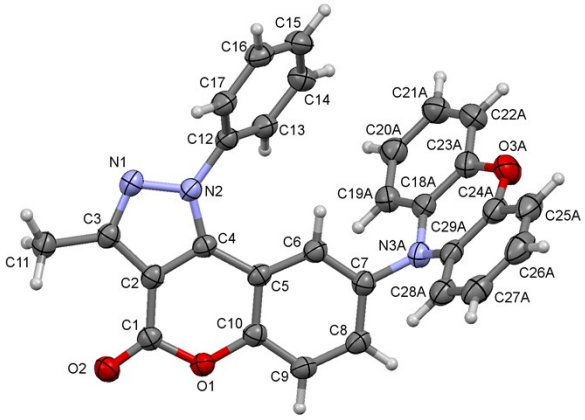

Figure SI5. X-ray structure of **POZCP**. Herein and thereafter, anisotropic displacement parameters are set to a 50% probability level.

The phenyl ring plane forms an angle of 52.37° with the chromenopyrazole core plane. The phenoxazine core is not planar: its side phenyl rings lie at an angle of 10.33° to each other, and the axis of bending of this fragment is the NC_4O ring. For that fragment, the maximum deviation from the plane reaches -13.8(2)° for the C24A-O3A-C23A-C18A angle, and the minimum is 12.54(17)° for the C29A-N3A-C18A-C23A angle.

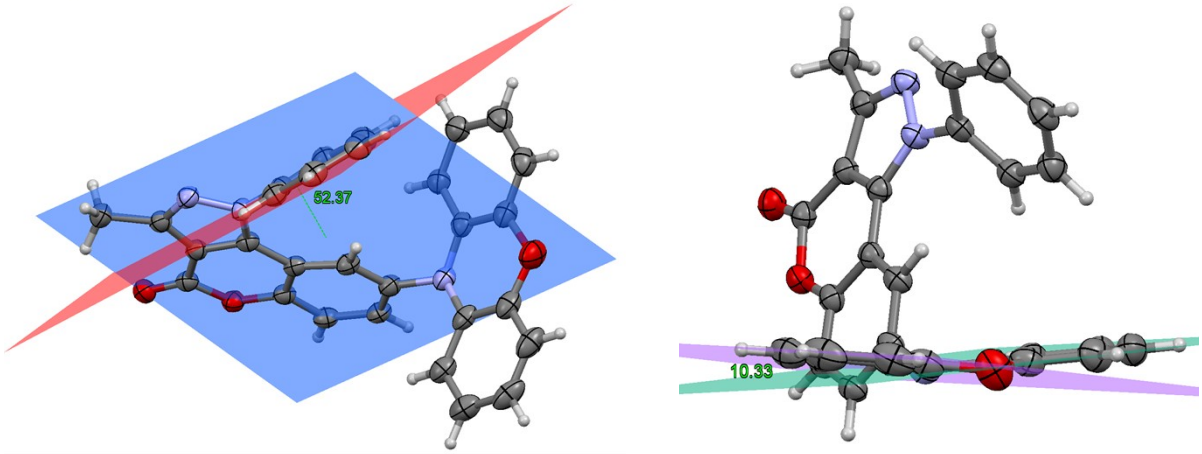

Figure SI6. The angle between the phenyl ring plane and the chromenopyrazole core plane (left) and the angle between the phenyl rings planes of the phenoxazine core (right) in **POZCP**.

In **PSZCP**, the deviation of the chromenopyrazole core is significantly smaller than in the **POZCP** structure. The maximum deviation is observed for the torsion angle C4-C5-C10-O1 which is 1.5(2)°, and the minimum is for the torsion angle N1-N2-C4-C2 which is -0.05(19)°. Nevertheless, the methyl group is more deviated: the torsion angle C1-C2-C3-C11 reaches a value of -1.8(3)° (when the similar angle in **POZCP** is -0.7(2)°).

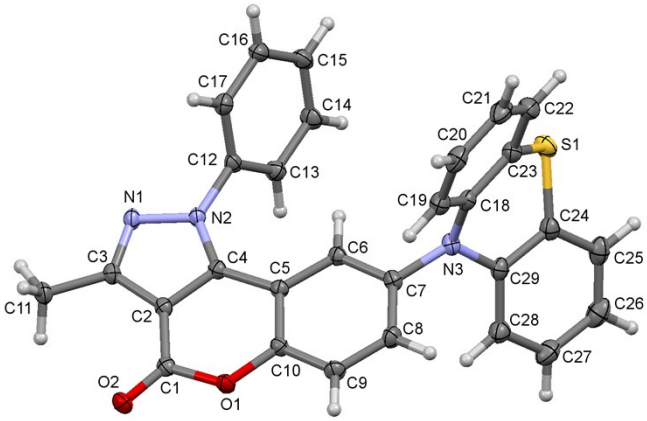

Figure SI7. X-ray structure of **PSZCP**.

The phenyl ring plane forms an angle of 69.46° with the chromenopyrazole core plane – which is greater than the observed in **POZCP**. The phenothiazine core is bent in the opposite direction compared to the **POZCP** structure. The side phenyl rings planes lie at an angle of 36.23° to each other. The bending of the NC_4S ring of the phenothiazine core is also greater, than the bending of the NC_4O ring: the maximum deviation from the plane reaches -35.76(15)° for the C24-S1-C23-C18 angle, and the minimum is -7.3(2)° for the S1-C24-C29-N3 angle. Such an increase in the ratio of bending for **PSZCP** compared to the **POZCP** is associated with an increase in the degree of freedom of the fragment due to long C-S bonds (the length of S1-C23 is 1.7611(19) Å, the length of S1-C24 is 1.7624(19) Å, while in **POZCP** the length of O3A-C23A is 1.3855(17) Å, and the length of O3A-C24A is 1.3844(19) Å).

It is noteworthy that in the **PSZCP** the geometry of the nitrogen atom N3 is flattened: the distance from the C7-C18-C29 plane to N3 is 0.177 Å, whereas in the **POZCP** structure the analogous distance is 0.258 Å, and the geometry of the nitrogen atom N3A is pyramidal.

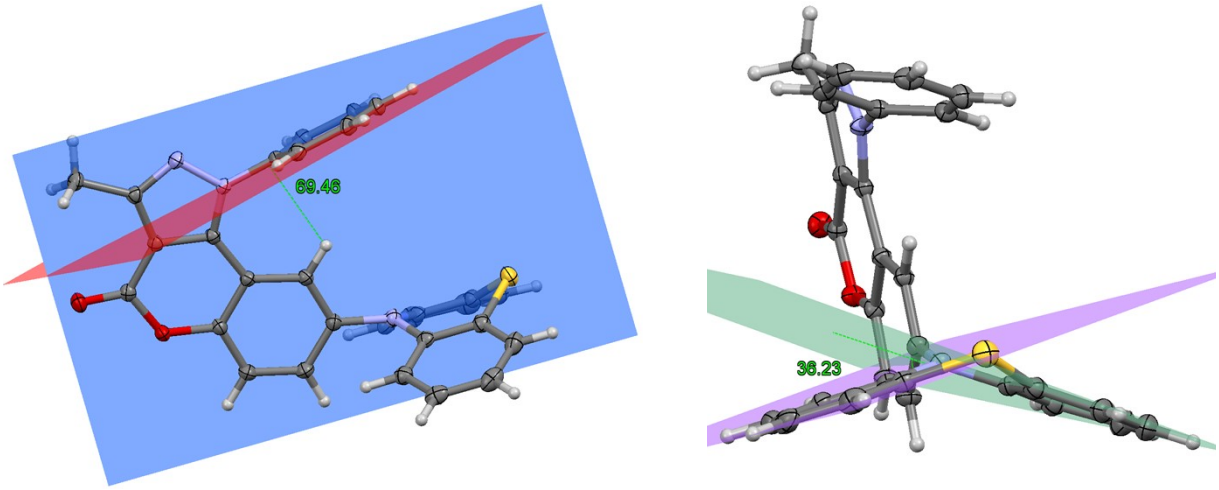

Figure SI8. The angle between the phenyl ring plane and the chromenopyrazole core plane (left) and the angle between the phenyl rings planes of the phenothiazine core (right) in **PSZCP**.

In **PSeZCP**, the deviation of the chromenopyrazole core is greater than in the **PSZCP**, but less than in the **POZCP**. The maximum deviation is observed for the torsion angle C10-O1-C1-C2 equal to 4.2(2)°, and the minimum is for the torsion angle C10-C5-C6-C7 equa The donor tricycle rotation relative to the chromenopyrazole core increases l to 0.0(2)°. In this case, the deviation of the methyl and carbonyl groups tends to zero.

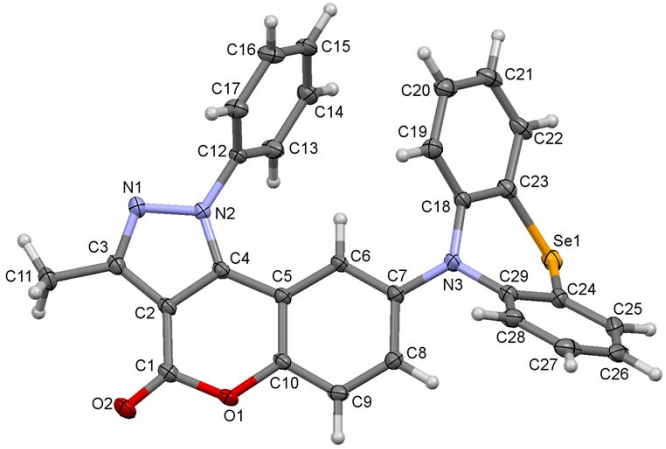

Figure SI9. X-ray structure of **PSeZCP**.

The rotation of phenyl ring is close to that in the **PSZCP** and reaches 72.85°. The phenoselenazine core is also bent similarly to the phenothiazine core in the **PSZCP**. The side phenyl rings lie at an angle of 57.04° to each other. It is noteworthy that the NC_4Se fragment of exhibits symmetry in the ratio of bending. The torsion angles of Se1 reach close values of 0.5(2)° and 0.6(2)°, and the torsion angles of N3 are -54.0(2)° and 53.4(2)°. The tendency of increasing the degree of fragment bending in the O-S-Se series, which was observed for the **POZCP** and **PSZCP** structures, is preserved. When the heteroatom is changed to Se, the degree of freedom of the fragment increases again due to the long C-Se bonds equal to 1.9123(18) Å and 1.9127(19) Å (in PSZCP, the S1-C23 length is 1.7611(19) Å, the

S1-C24 length is 1.7624(19) Å, in **POZCP**, the O3A-C23A length is 1.3855(17) Å, the O3A-C24A length is 1.3844(19) Å).

The geometry of N3 in the **PSeZCP** becomes distinctly planar: the distance from the C7-C18-C29 plane to N3 reaches 0.066 Å, and this value is significantly smaller than in the **PSZCP** and **POZCP**.

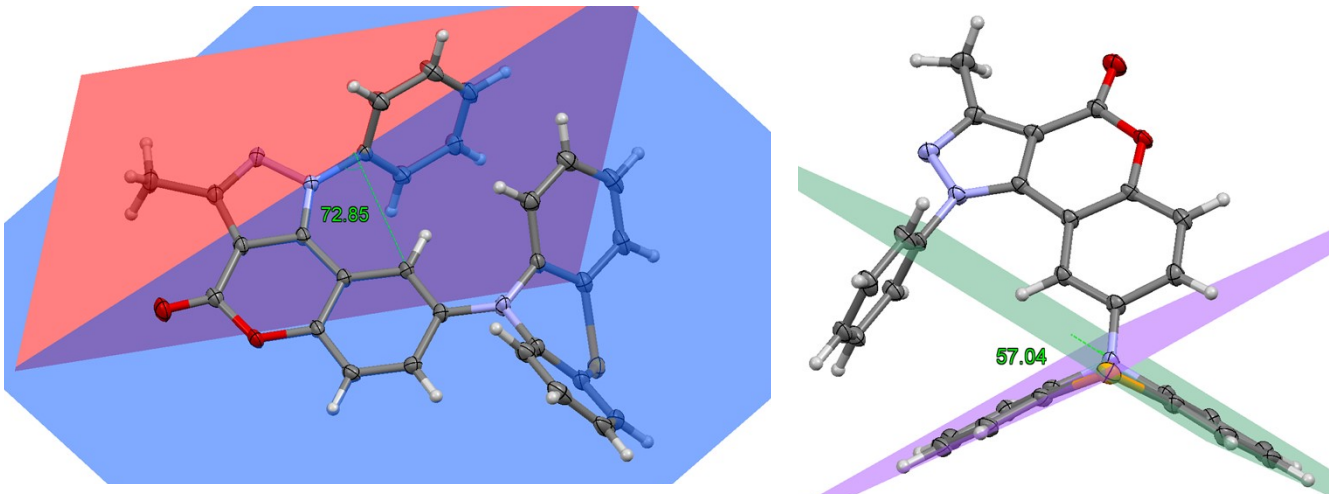

Figure SI10. The angle between the phenyl ring plane and the chromenopyrazole core plane (left) and the angle between the phenyl rings planes of the phenoselenazine core (right) in **PSeZCP**.

The **POZPhCP** differs from the **POZCP** by the presence of a phenyl ring as a linker between the chromenepyrazole and phenoxazine cores. It is noteworthy that, despite the similarity of the compound to **POZCP**, in the **POZPhCP** the deviation of the chromenepyrazole core is significantly smaller than in the **POZCP**. The maximum deviation is observed for the C1-C2-C4-C5 torsion angle equal to -1.8(3)°, and the minimum is for the N1-N2-C4-C2 torsion angle equal to -0.1(2)°. The deviation of the chromenepyrazole core increases in the series of structures **PSZCP-POZPhCP-PSeZCP-POZCP**. The deviation of the methyl and carbonyl groups is close to those in the **PSZCP** structure: the torsion angle C1-C2-C3-C11 reaches a value of -1.6(4)°, and the torsion angle O2-C1-C2-C3 is 2.3(4).

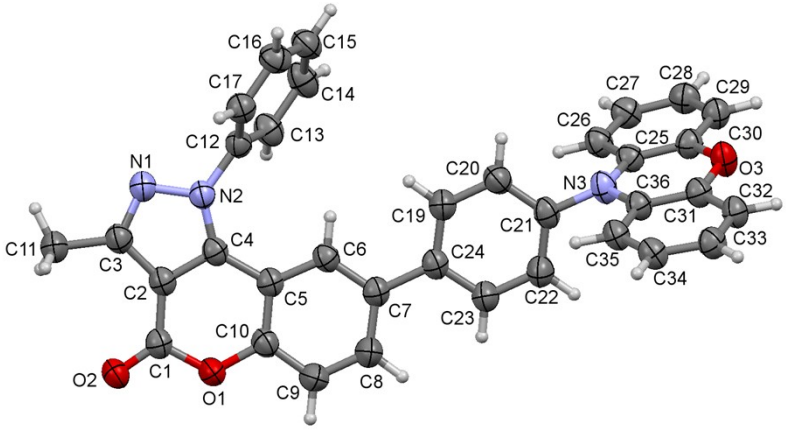

Figure SI11. X-ray structure of **POZPhCP**.

The phenyl ring plane forms an angle of 64.31° with the chromenopyrazole core plane, hence the degree of rotation of this fragment increases in the series of structures **POZCP-POZPhCP-PSZCP-PSeZCP**. The phenoxazine core demonstrates an approach to a planar conformation, the angle between the planes of its side phenyl rings reaches only 6.26°. The rotation of the phenoxazine core relative to the linker is equal to 75.90°. The linker itself also tends to a planar conformation relative to the chromenopyrazole core, forming a torsion angle C8-C7-C24-C23 equal to 7.4(3)°. The linker reduces the influence of the chromenopyrazole core on the phenoxazine core. The geometry of N3 in the **POZPhCP** is close to the geometry of N3 in **PSZCP**: the distance from the C21-C25-C36 plane to N3 reaches 0.123 Å, hence the transition of N3 geometry from pyramidal to planar occurs in the series of structures **POZCP-PSZCP-POZPhCP-PSeZCP** with a pronounced change between the **POZCP** and **PSZCP** structures.

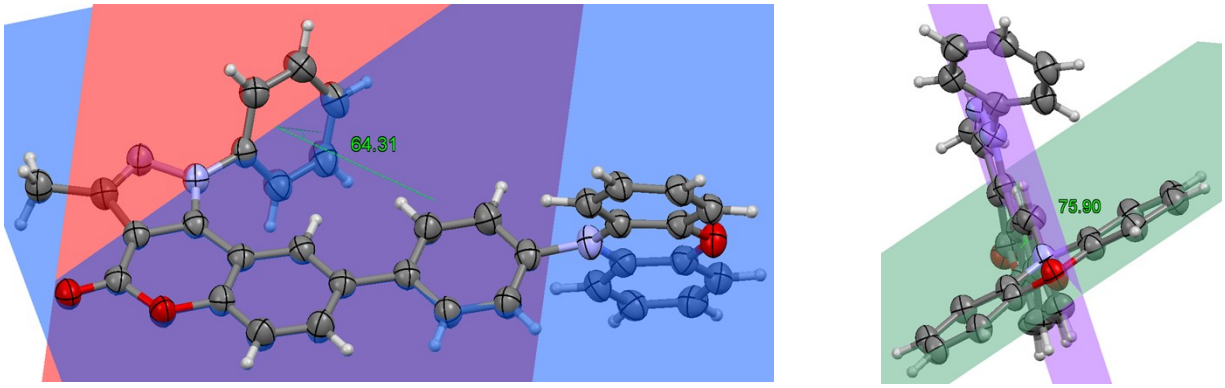

Figure SI12. The angle between the phenyl ring plane and the chromenopyrazole core plane (left) and the angle between the linker plane and the phenoxazine core plane (right) in **POZPhCP**.

SI-3 CV measurements

Cyclic voltammograms of the new choromophores **POZCP, PSZCP, PSeZCP** and **POZPhCP** were obtained on a glassy carbon electrode in a DMF solution containing tetrabutylammonium tetrafluoroborate as a supporting electrolyte. The electroreduction (ER) peaks of both compounds are quasi-reversible at a potential superposition rate of 0.1 Vs^{-1}, while the electro-oxidation (EO) peaks are irreversible up to a sweep rate of 5 Vs^{-1}.

In order to estimate the values of the frontier orbitals, the potentials of the onset of the ER (E^{red}_{onset}) and EO (E^{ox}_{onset}) peaks were determined from the obtained curves relative to the potential of the reversible oxidation of ferrocene Fc/Fc^+, used as an internal standard. Taking into account that the value of the absolute oxidation potential of ferrocene is -5.1 V [1, 2], the energies of the lowest free (E_{LUMO}) and highest occupied orbitals (E_{HOMO}) were calculated using the equations:

$$E_{HOMO}\ (eV) = -|e|(\ E^{ox}_{onset,\ Fc/Fc+} + 5.1) \qquad (1)$$

$$E_{LUMO}\ (eV) = -\ |e|(\ E^{red}_{onset,\ Fc/Fc+} + 5.1) \qquad (2)$$

The results are presented in the **Table SI6**.

Table SI6. Electrochemical properties of the choromophores **POZCP, PSZCP, PSeZCP** and **POZPhCP, PSZPhCP, PSeZPhCP** in DMF solution

Compound	E^{red}_{onset} (vs Fc/Fc^+)[a], V	E_{LUMO}[b], eV	E^{ox}_{onset} (vs Fc/Fc^+)[a], V	E_{HOMO}[b], eV	E_g[c], eV
POZCP	-2.19	-2.91	0.24	-5.34	2.43
PSZCP	-2,21	-2,89	0.26	-5.36	2.47
PSeZCP	-2.25	-2.85	0.26	-5.36	2.51
POZPhCP	-2.31	-2.79	0.24	-5.34	2.55

[a] Here E^{ox}_{onset} and E^{red}_{onset} are oxidation and reduction peak potential relative to Fc/Fc^+ respectively.

[b] Energies of frontier orbitals were calculated by equations (1) and (2) and by quantum chemistry with the use of B3LYP functional

[c] $E_g = E_{LUMO} - E_{HOMO}$

We estimated E_G of **POZCP, PSZCP, PSeZCP** and **POZPhCP** compounds as 2.43, 2.47, 2.51 and 2.55 eV, respectively.

SI-4 Photophysical parameters

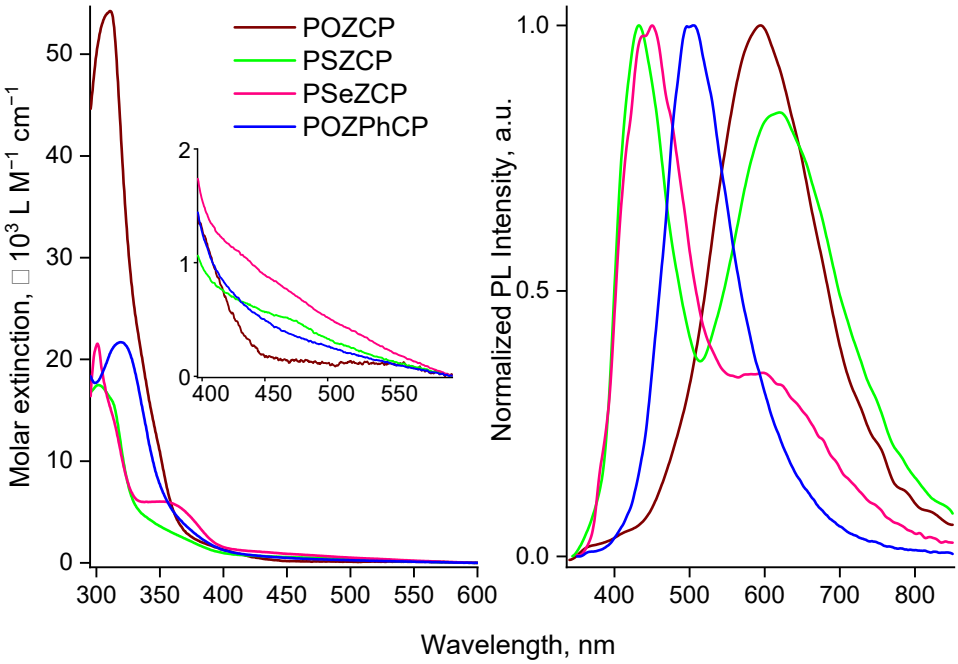

Figure SI13. Absorption (left) and normalized fluorescence (right) spectra of DCM dissolved **POZCP**, **PSZCP**, **PSeZCP** and **POZPhCP** dyes.

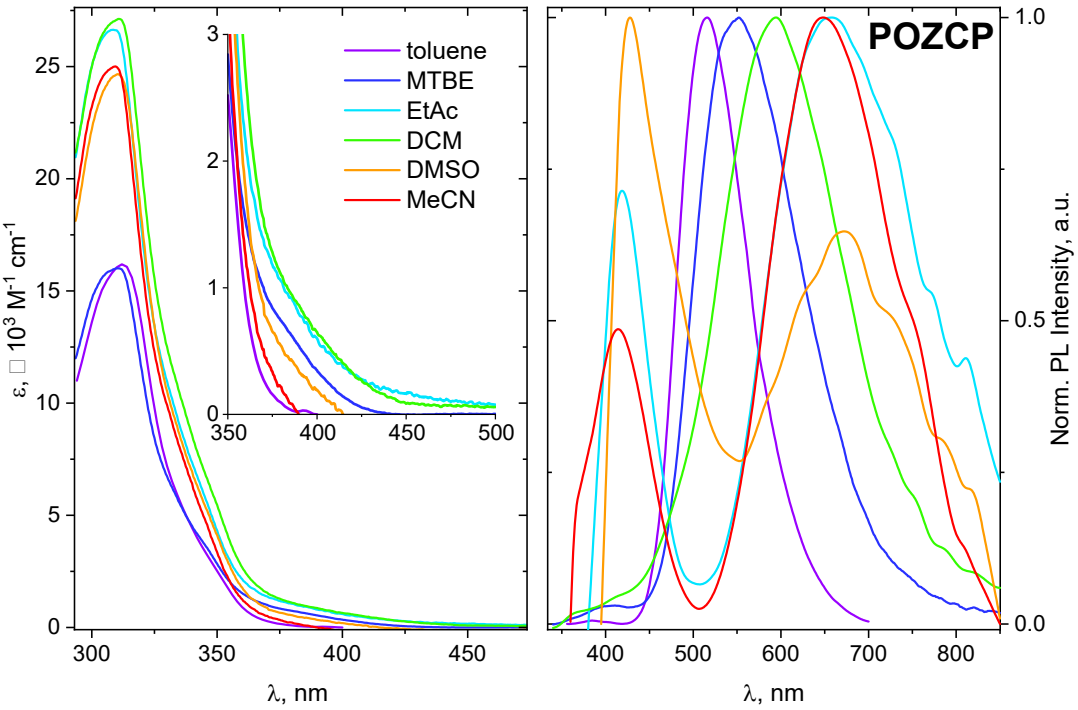

Figure SI14 (a) UV-vis (left) and normalized fluorescence (right) spectra of **POZCP** dyes dissolved in toluene, MTBE, EtAc, DCM, DMSO and MeCN.

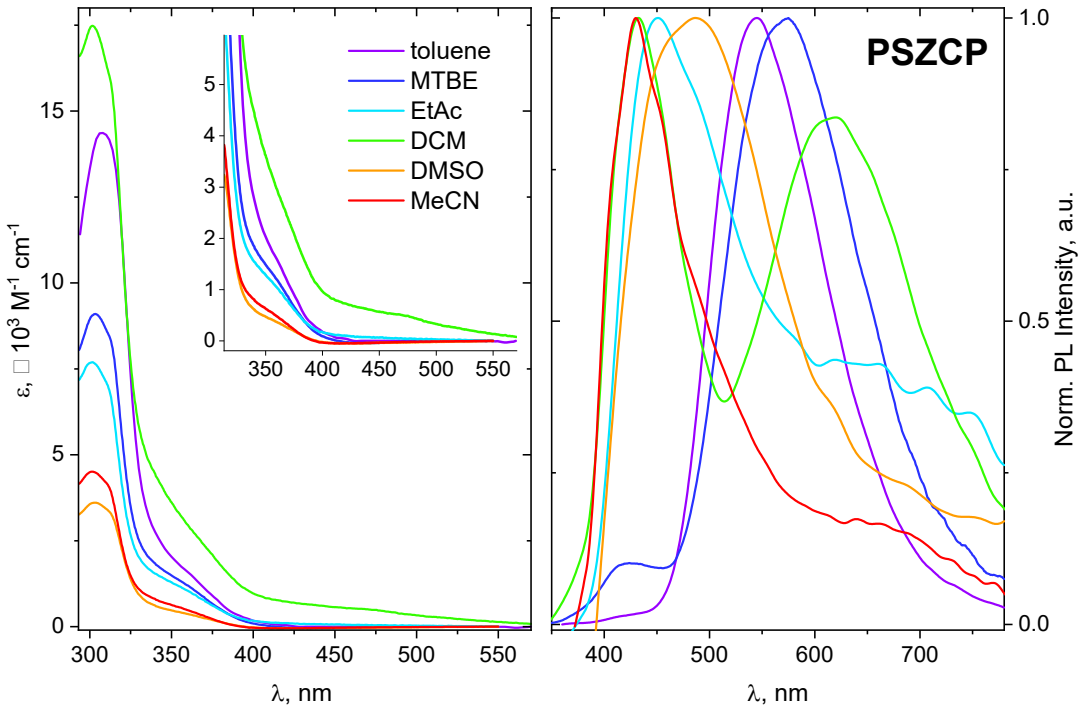

Figure SI14 (b) UV-vis (left) and normalized fluorescence (right) spectra of **PSZCP** dyes dissolved in toluene, MTBE, EtAc, DCM, DMSO and MeCN.

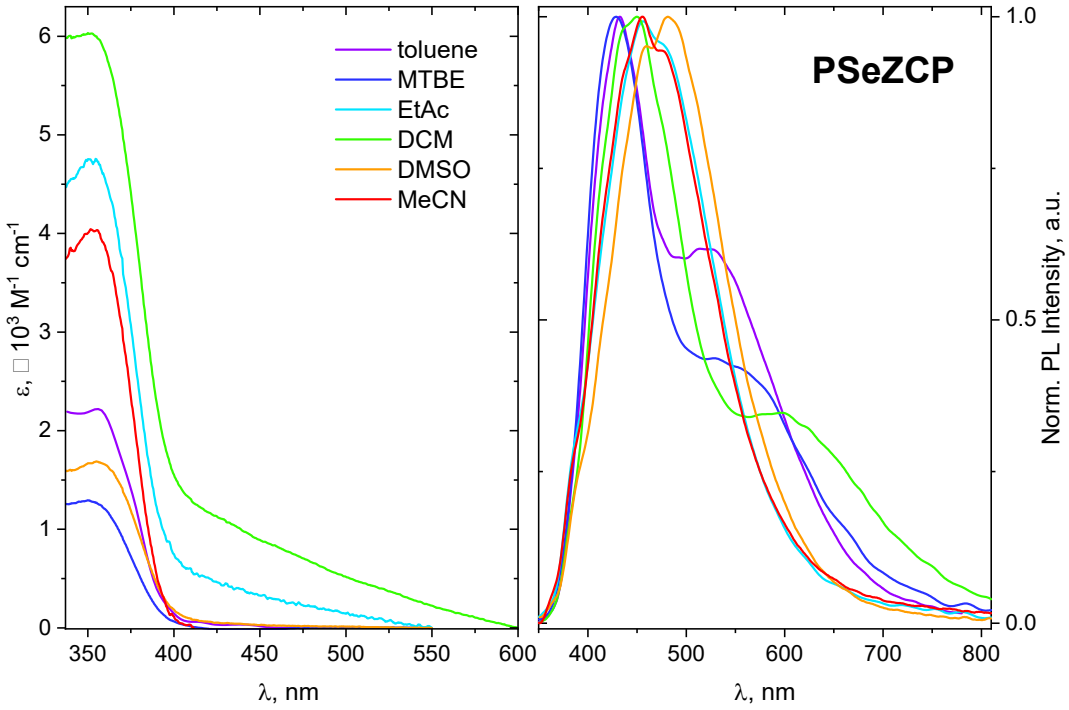

Figure SI14 (c) UV-vis (left) and normalized fluorescence (right) spectra of **PSeZCP** dyes dissolved in toluene, MTBE, EtAc, DCM, DMSO and MeCN.

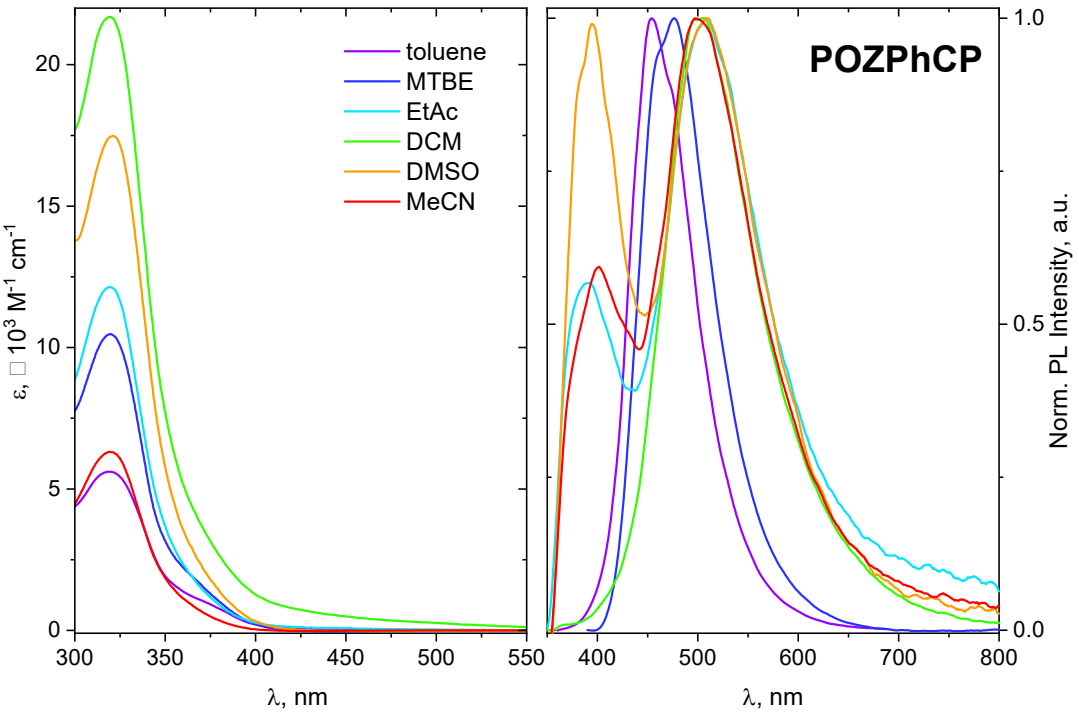

Figure SI14 (d) UV-vis (left) and normalized fluorescence (right) spectra of **POZPhCP** dyes dissolved in toluene, MTBE, EtAc, DCM, DMSO and MeCN.

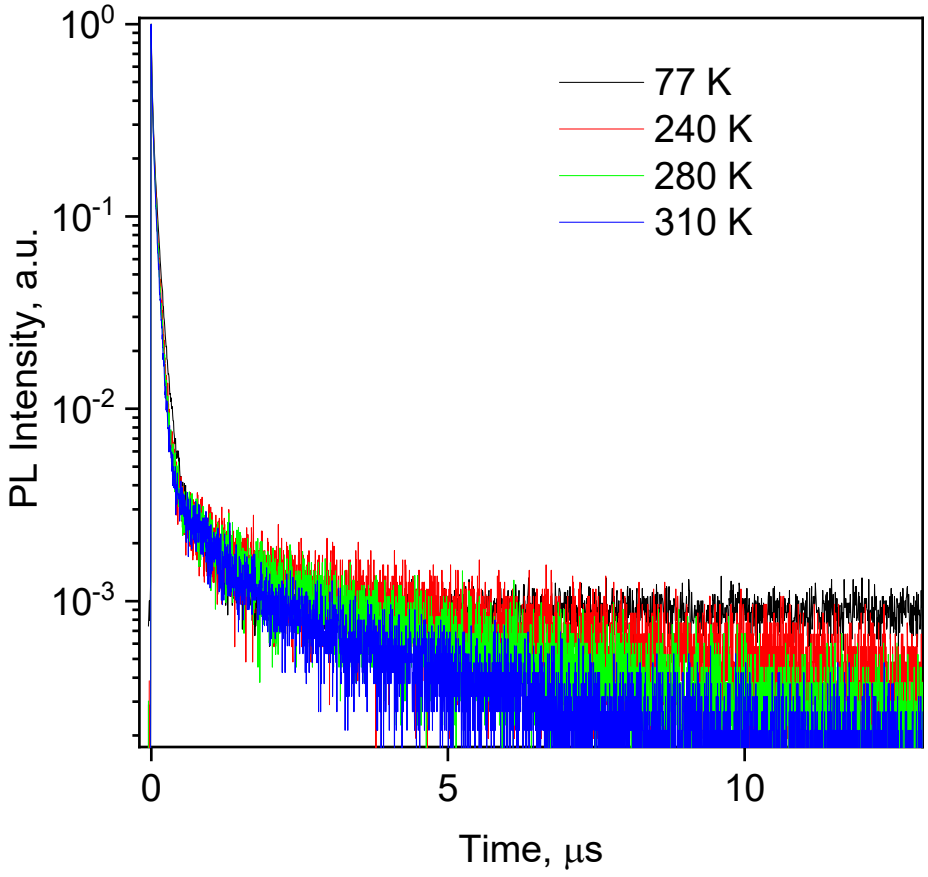

Figure SI14 (e) PL decay for POZCP doped into PMMA measured at 77, 240, 280 and 310 K (λ_{exc} = 376 nm, λ_{reg}=540 nm)

Estimation of the rate constants

Rate constants were determined from the measurements of quantum yields and lifetimes of fluorescence and TADF components according to the equations

$$k_{rad}=\Phi_p/\tau_p \quad (1)$$

$$\Phi=k_{rad}/(k_{rad}+k_{nrad}) \quad (2)$$

$$k_{nrad}= k_{rad}\cdot(1/\Phi-1)$$

$$k_{ISC}=(1 - \Phi_p)/\tau_p \quad (3)$$

$$\Phi_{nrad}= k_{nrad}/(k_{rad}+ k_{nrad}+ k_{ISC}) \quad (4)$$

$$\Phi_{ISC}=1- \Phi_p- \Phi_{nrad}= k_{ISC}/(k_{rad}+ k_{nrad}+ k_{ISC}) \quad (5)$$

$$k_{del}=\Phi_{del}/(\Phi_{ISC}\cdot\tau_{del}) \quad (6)$$

$$k_{RISC}= \Phi_{del} / (k_{ISC}\cdot\tau_p\cdot\tau_{del}\cdot\Phi_p) \quad (7)$$

Φ_{nrad} –efficiency of non-radiative processes, Φ_{ISC} – efficiency of intersystem crossing process

Table SI7 (a). Photophysical parameters obtained for dyes dissolved in different solvents: peak of the long-wavelength gauss in absorption spectrum λ_{ICT}, maximum molar extinction coefficient ε_{max}, emission maximum wavelength λ_{FLUO}, full width half-maximum FWHM for the emission bands, Stokes shift $\Delta\nu$, energy of the first excited singlet state $E(S_1)$.

Dye	Solvent	λ_{ICT}, nm	$\varepsilon_{max}\times10^3$, $M^{-1}\cdot cm^{-1}$	λ_{FLUO}, nm	FWHM, nm	$\Delta\nu$, 10^3 cm^{-1}	$E(S_1)$ eV
POZCP	toluene	342	16.3	516	94	9.9	2.76
	MTBE	369	16.0	548	139	8.9	2.84
	EtAC	338	26.3	419, 656	60, 203	14.3	2.45
	DCM	380	27.2	595	164	9.5	2.20
	DMSO	358	24.6	428, 672	89, 196	13.1	2.38
	MeCN	365	25.1	414, 648	83, 171	12.0	2.96
PSZCP	toluene	334	14.3	545	124	11.6	3.03
	MTBE	344	9.1	420, 573	65, 148	11.6	2.45
	EtAC	334	7.7	450	153	7.7	2.95
	DCM	400	17.5	431, 616	87, 152	8.8	2.37
	DMSO	338	3.6	486	165	9.0	2.70
	MeCN	336	4.5	430*, 651	98, 172	14.4	3.06
PSeZCP	toluene	375	2.2	432, 532	67, 156	7.9	3.28
	MTBE	366	1.3	429, 557	92, 195	9.4	3.06
	EtAC	365	4.7	456	133	5.5	2.78
	DCM	369	6.0	447, 601	100, 194	10.5	2.33

	DMSO	368	1.7	481	135	6.4	2.57
	MeCN	365	4.1	454	131	5.4	3.10
POZPhCP	toluene	392	5.7	454	74	5.0	2.79
	MTBE	354	10.5	476	83	8.7	3.00
	EtAC	326	12.1	390, 510	61, 122	12.0	3.11
	DCM	352	21.7	509	109	9.7	2.65
	DMSO	349	17.5	394, 508	80, 126	9.3	2.62
	MeCN	347	6.4	401, 499	79, 118	8.3	3.15

Table SI7 (b). Efficiency of prompt fluorescence (Φ_p), delayed fluorescence (Φ_{del}), intersystem crossing process (Φ_{ISC}) and non-radiative relaxation process (Φ_{nrad}) obtained for dyes for the dyes doped in PMMA of 10wt%.

Dye	Φ_p %	Φ_{del} %	Φ_{ISC} %	Φ_{nrad} %
POZCP	6.3	4.2	61.0	34.9
PSeZCP	2.9	2.6	65.1	33.0
POZPhCP	9.1	4.9	58.4	35.8

Table SI7 (c). Lifetimes for **POZCP** doped into PMMA measured in degassed atmosphere upon 360 nm at temperature region of 77-310 K

Temperature, K	τ_p, ns	τ_{del}, ns
78	69	246
100	73	346
140	82	645
160	81	736
180	93	1697
200	74	2543
220	101	2631
240	76	2719
250	78	2643
260	74	2292
280	74	2062
290	71	1818
300	73	1787
310	67	1522

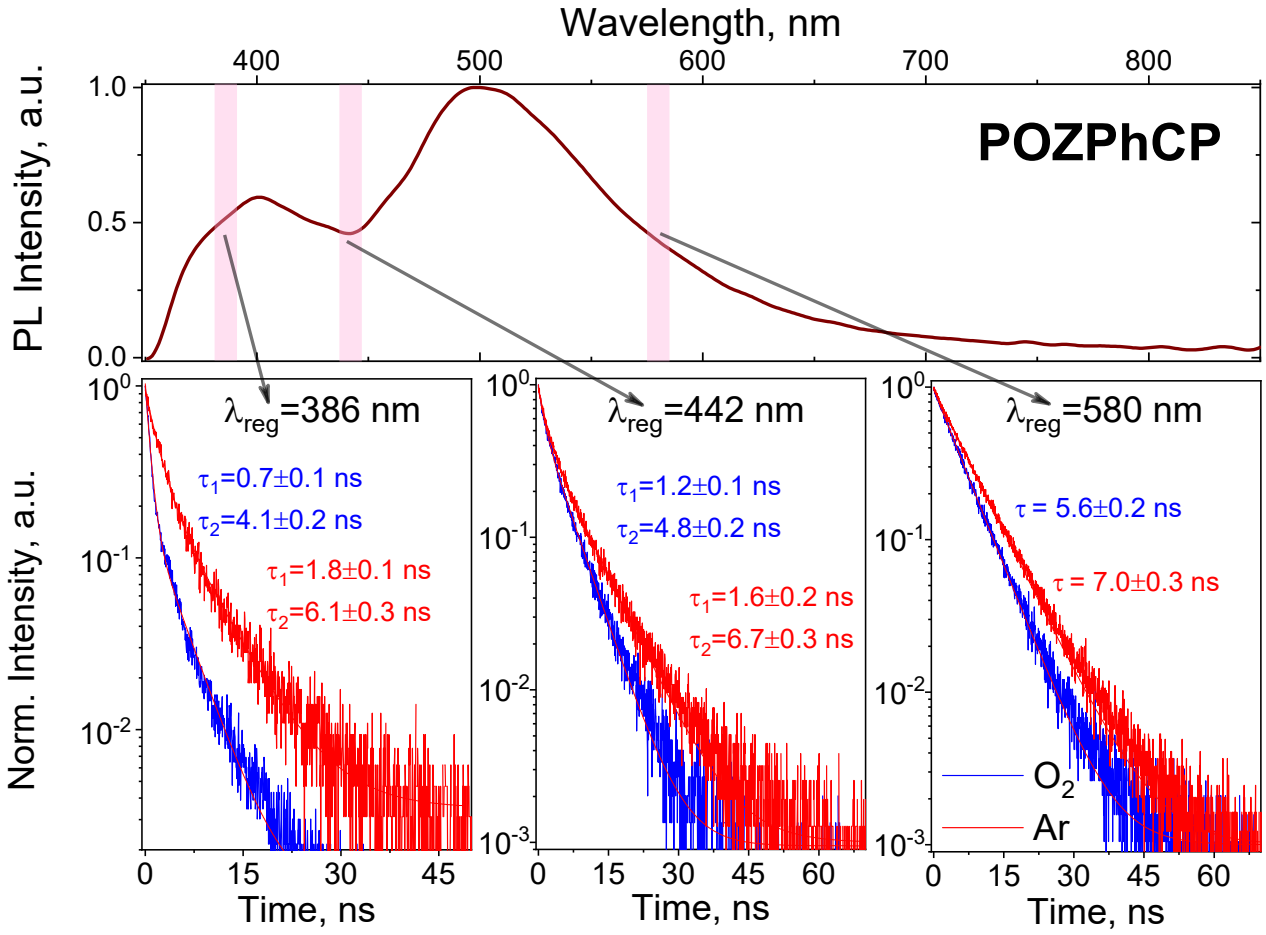

Figure SI15. top: Normalized PL spectrum of MeCN dissolved **POZPhCP** dye; **bottom:** PL decays recorded for aerated (blue curve) and degassed (red curve) solution upon excitation at 376 nm registered at 386 nm, 442 nm and 580 nm at 300 K.

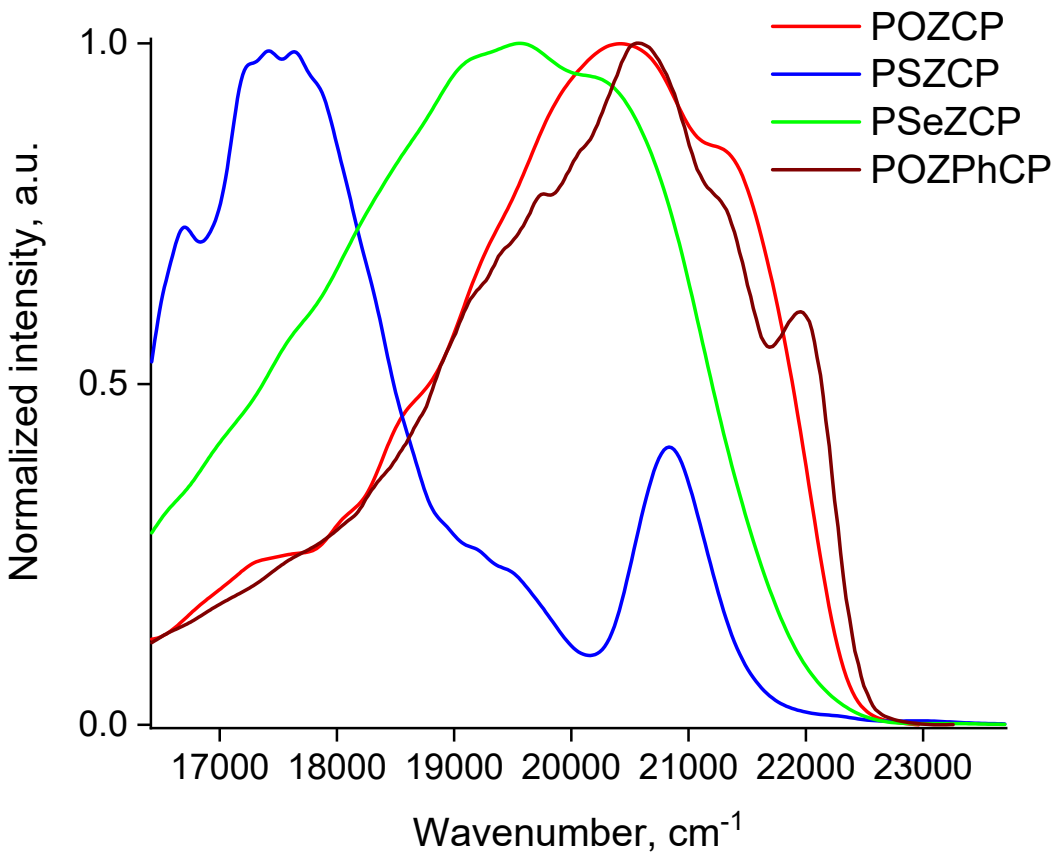

Figure SI16. Normalized phosphorescence spectra of toluene dissolved **POZCP**, **PSZCP, PSeZCP** and **POZPhCP** dyes recorded upon excitation at 340 nm with time delay 100 us at 77 K.

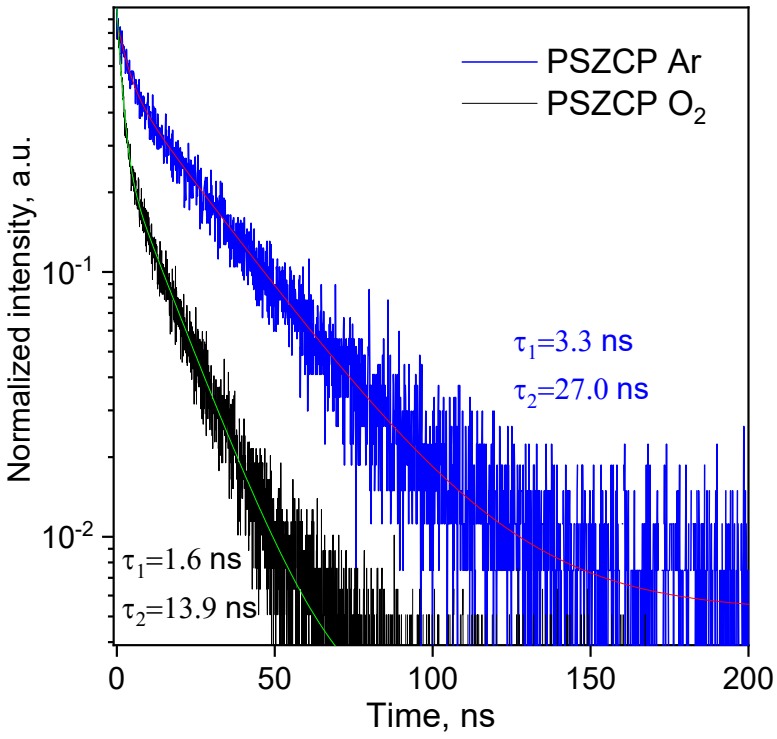

Figure SI17. PL decay for toluene dissolved **PSZCP** dye in aerated (black curve) and degassed (blue curve) atmosphere upon excitation at 376 nm recorded at 540 nm at 300 K.

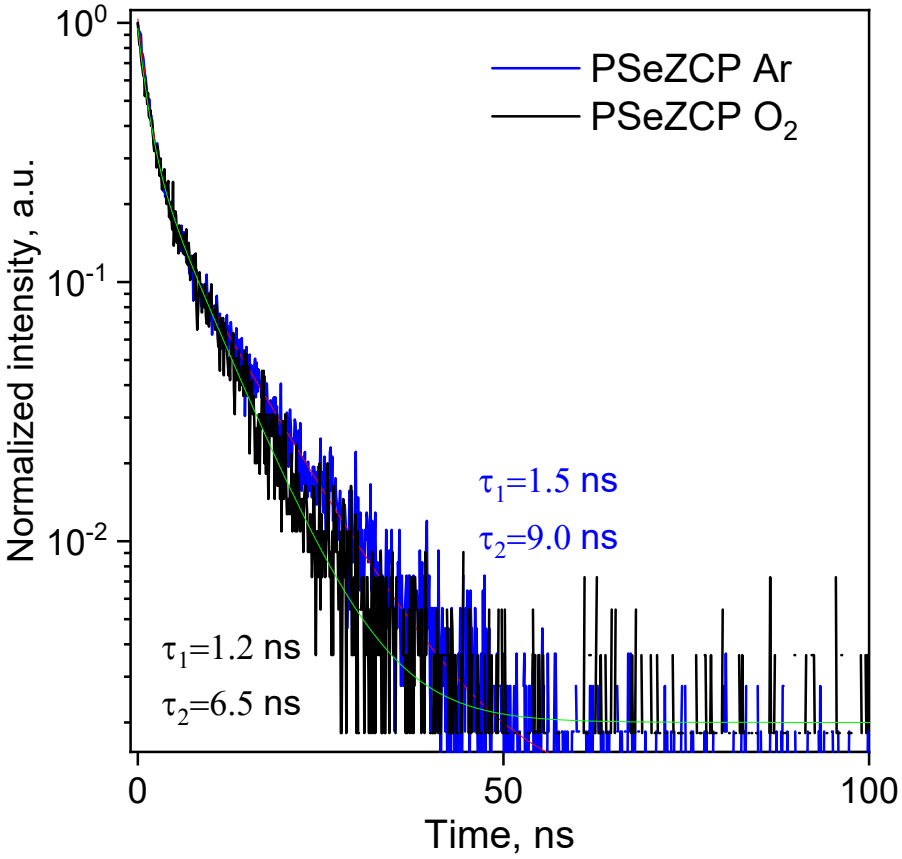

Figure SI18. PL decay for toluene dissolved **PSeZCP** dye in aerated (black curve) and degassed (blue curve) atmosphere upon excitation at 376 nm recorded at 540 nm at 300 K.

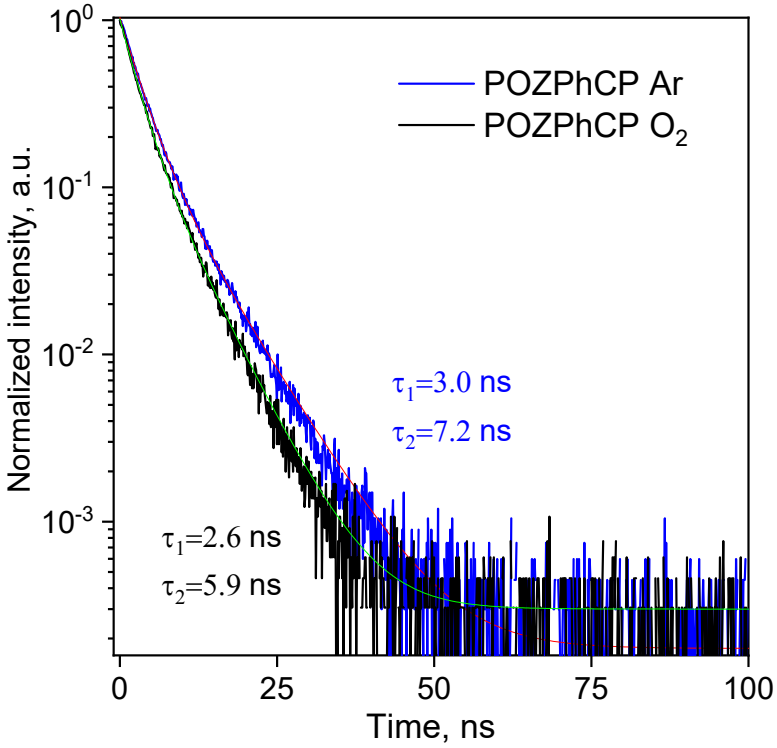

Figure SI19. PL decay for toluene dissolved **POZPhCP** dye in aerated (black curve) and degassed (blue curve) atmosphere upon excitation at 376 nm recorded at 540 nm at 300 K.

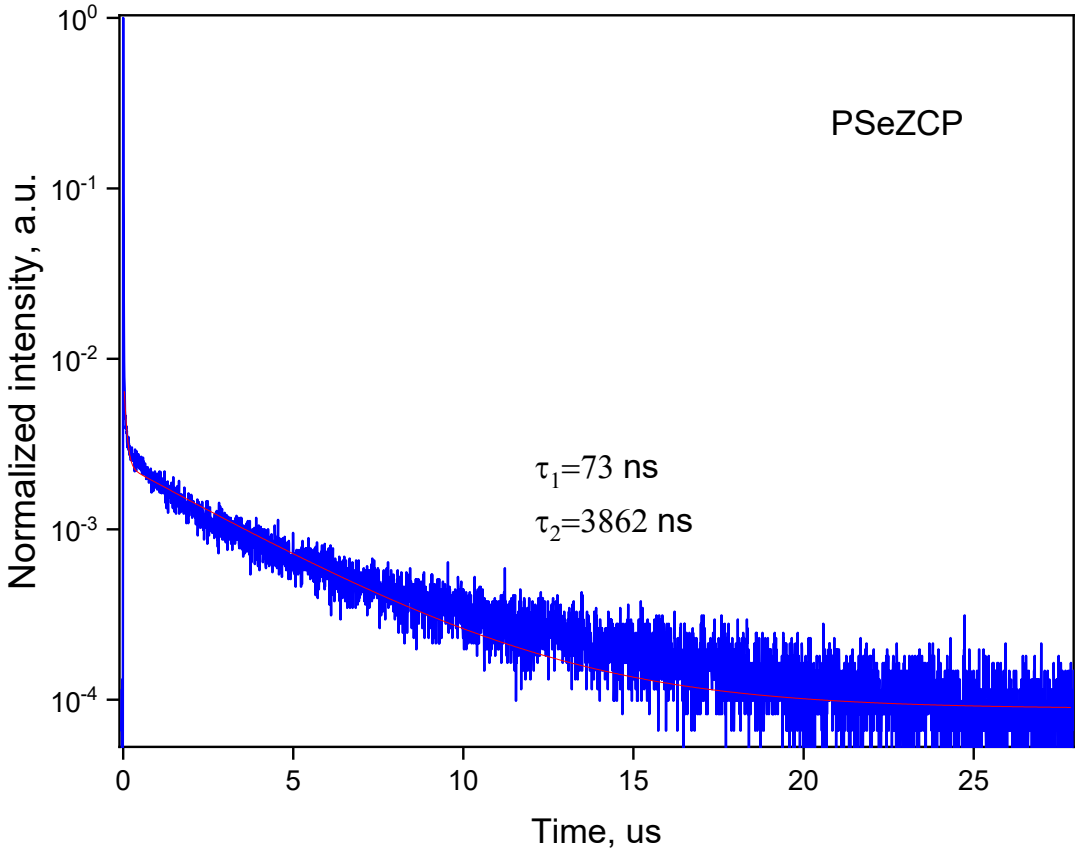

Figure SI20. PL decay for **PSeZCP** dye in thin film upon excitation at 376 nm recorded at 540 nm at 300 K.

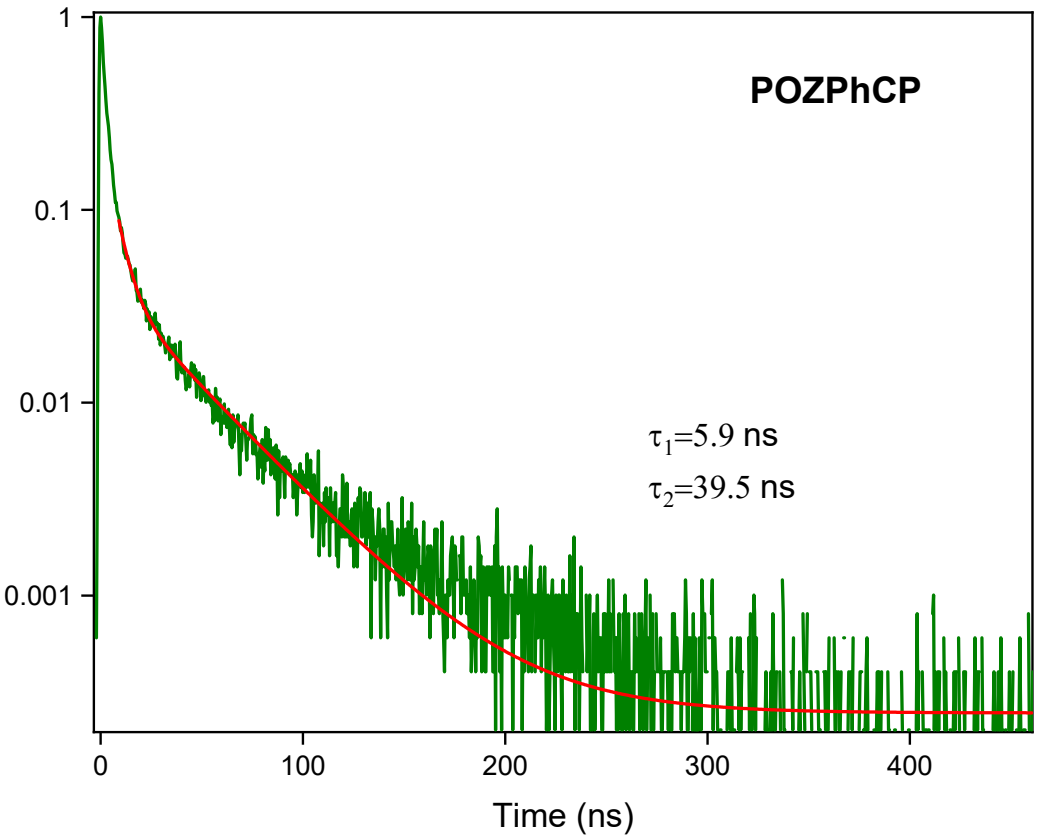

Figure SI21. PL decay for **POZPhCP** dye in thin film upon excitation at 376 nm recorded at 540 nm at 300 K.

SI-5 Quantum-chemical calculations

Table SI8. Quantum-chemical calculations results.

$\mu(S_0)$, Debye.	$\mu(S_1)$ relax, D.	$\Delta\mu(S_{1\ relax}\text{-}S_0)$, D.	${}^{R}D_{CT}$, Ang.	q_{CT} (transferred charge) A.u.
4.04	21.64	17.6	3.156	1.216

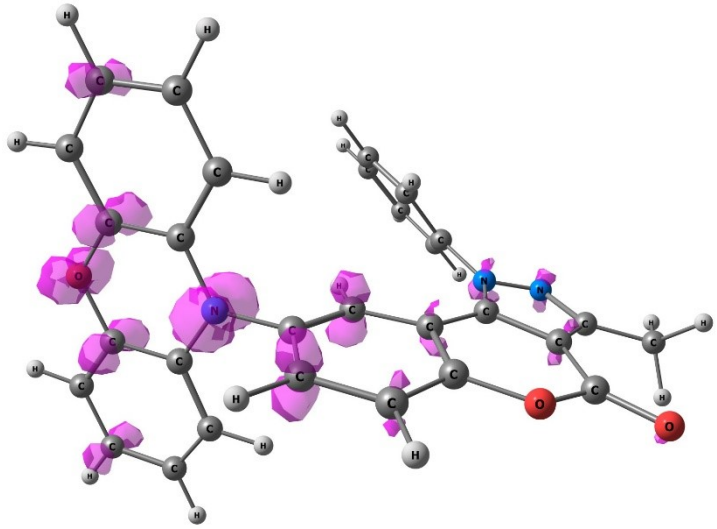

Figure SI22. Spin density plot (at T_1 geometry).

SI-6. Comparison of data reported for several representative sky-blue TADF emitters

Table SI9. OLED performances of reported sky-blue TADF emitters

Name	**Structure**	**PL-QYs, %**	**Egap, eV**	**EQE, %**	**λ_{max}EL, nm**	**Reference**
DMAC-TRZ	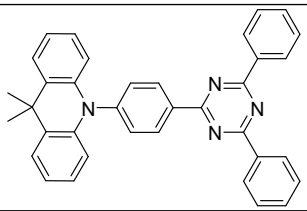	83	3	26.5	495	10.1039/C5CC05022G
HCB-3	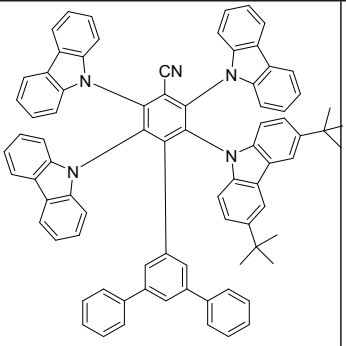	92	3.35	24.1	492	10.1039/D4TC05347H

ACRSA	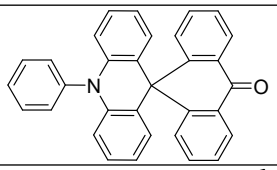	45	-	16.4	486	10.1039/C3CC44179B.
1MPA	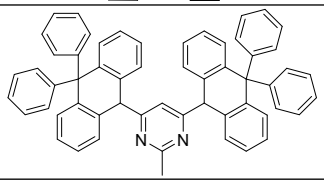	70	3.55	13.6	491	10.1039/D1TC03598C
DtBuCzB	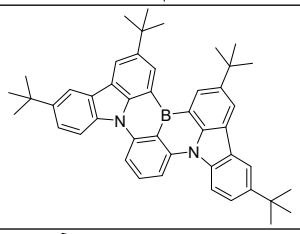	91	2.55	21.6	488	10.1002/adom.201902142
AcCBz	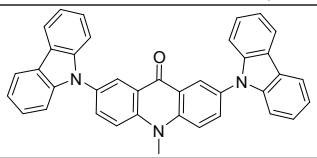	60	2.93	-	465	10.1021/acs.jpcc.8b08357
PerTz1	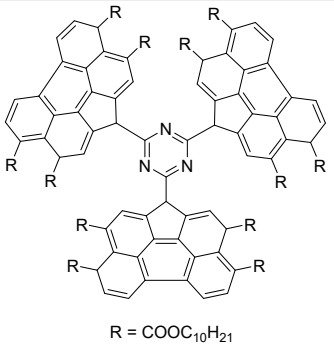	-	2.34	1.8	535	10.1002/ejoc.201800161
TDBA-Ac	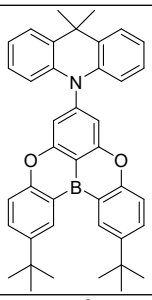	93	3	21.5	465	10.1038/s41566-019-0415-5.
TZ	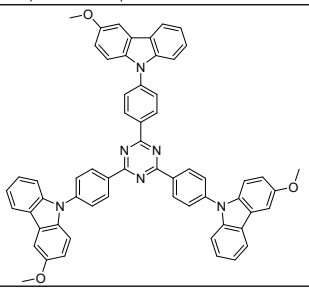	32	2.89	1.1	520	10.1039/c6tc03063g

DMAC-DPS	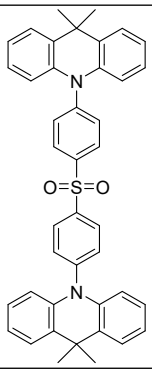	68	3	12.2	505	10.1039/C6TC00418K

SI-7. EQE of devices with TADF emitters

At lower dye contents, a short-wavelength band belonging to the host appeared in the EL spectra, and with its increase, concentration quenching was present. In both cases, a decrease in the maximum current (CE), luminous efficiency (PE), external quantum efficiency (EQE) and brightness was observed.

The TAZ molecule contains a triazole moiety, which provides high electron mobility of 10^{-4} $cm^2V^{-1}s^{-1}$,[38] in addition, the position of its LUMO energy level (–2.7 eV) coincides with the corresponding level of TmPyPb (Figure 9, a), which ensures barrier-free transition of electrons to the EML and movement towards the EML/HTL boundary, where recombination with holes occurs.

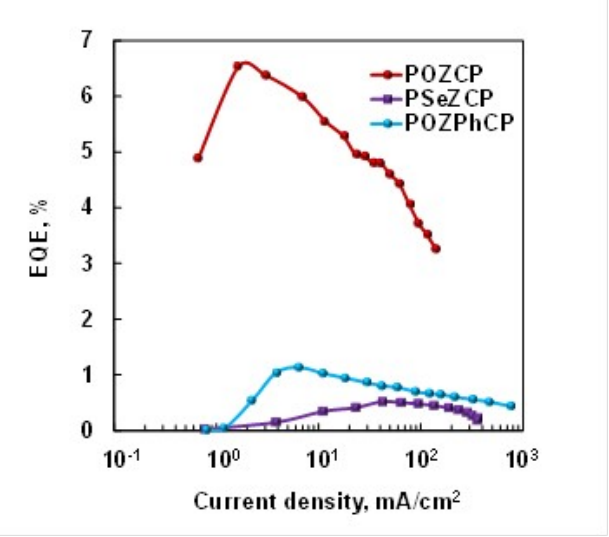

Figure SI23. Dependence of EQE on the current density of OLEDs with emissive layers containing dyes in a CBP host possessing TADF. The dye content in all EMLs was 17 wt%.

The OLED based on a blue TADF emitter, 10,10’ (sulfonylbis(4,1-phenylene))bis(9,9-dimethyl-9,10-dihydroacridine) (DMAC-DPS, achieved a maximum EQE as high as 19.5% but the T50 (time to 50% of initial luminance) was only 1 h at an initial luminescence of 500 cd m^2 [3].

The luminance of OLEDs based on 2,6-bis(3,6-diphenyl-9H-carbazol-9-yl)-9H-xanthen-9-one

(23PCX), and 3,6-bis(3,6-diphenyl-9H-carbazol-9-yl)-9H-xanthen-9-one (33PCX) as a function of operational time under constant current density at an initial luminance (L_0) of 1000 cd m^{-2} LT_{95} ≈13 and ≈15 h The LT_{95} of those devices at an initial luminance of 100 cd m^{-2} can be extrapolate in ≈650 h for 33PCX and ≈750 h for 23 PCX-based devices.[4]

Recently, substantial efforts have been devoted on improving the operation lifetimes of devices based on v-DABNA as emitter by developing stable TADF sensitizers. And the LT_{95}s of ≈18 h and <10h at initial luminance of 1000 cd m^{-2} have been obtained by Adachi's group and Lee's group, respectively**.**

References

1. Cardona, C.M.; Li, W.; Kaifer, A.E.; Stockdale, D.; Bazan, G.C. Electrochemical Considerations for Determining Absolute Frontier Orbital Energy Levels of Conjugated Polymers for Solar Cell Applications. Adv. Mater. 2011, 23, 2367–2371, doi:10.1002/adma.201004554.
2. Bujak, P.; Kulszewicz-Bajer, I.; Zagorska, M.; Maurel, V.; Wielgus, I.; Pron, A. Polymers for electronics and spintronics. Chem. Soc. Rev. 2013, 42, 8895, doi:10.1039/c3cs60257e
3. D. Zhang, M. Cai, Y. Zhang, D. Zhang and L. Duan, Mater. Horiz., 2016, **3**, 145–151.
4. Zhang, D., Wada, Y., Wang, Q., Dai, H., Fan, T., Meng, G. & Kaji, H. (2022). Highly efficient and stable blue organic light-emitting diodes based on thermally activated delayed fluorophor with donor-void-acceptor motif. *Advanced Science*, *9*(12), 2106018.